Response to Reviewer 1 to the paper : Theoretical investigation of mixing in warm clouds – Part 2: Homogeneous mixing authored by M. Pinsky, A. Khain, A. Korolev, and L. Magaritz-Ronen

Authors appreciate the Reviewer's time and efforts to review our manuscript.

General comments to all three parts (repeated in all three reviews). I read the papers with considerable interest mostly because this seemed to be a popular topic some time ago, in both observations and modeling. I was curious to see what new these manuscripts bring. Frankly, I was disappointed. First, the analysis concerns a highly idealized problem, with little applications to real clouds. Turbulent mixing in clouds is by far more complicated that situations depicted in Fig. 1 of part 1 (and then repeated in different shapes as Figs. 1 in Part 2 and 3). Second, I am aware of study in which the authors developed a fairly sophisticated model of microphysical evolution during turbulent stirring (Jarecka et al., JAS 2013) aiming at prediction of the homogeneity of mixing. They applied the model to LES simulations of shallow convective cloud field. The impact was surprisingly small and the authors of that paper argued why this might be so (the entrained air comes from the descending shell and is not far from saturation). So in a sense the subject is "old news". Finally, the lengthy discussions, full of unnecessary caveats and references to details of small multi-panel figures, made the reading frustrating. All three parts read like a student dissertation, not a concise scientific paper highlighting key points and leaving the rest for the reader to follow. Thus, I read the manuscripts with decreasing interest, and my comments are more detailed for the part 1, and get more general for parts 2 and 3.

Overall, I do not believe that the subject matter deserves close to 100 pages and close to 50 figures. I feel that the material deserves a single, short and concise manuscript, with new material clearly separated from what I feel has been discussed in the past, perhaps not at such a level of detail. Reading introductions to all three parts made me mad, because all three say basically the same thing with different language and organization. Part 1 is mostly trivial in my view, with some parts speculative and other repeating already published material (see detailed comments). Parts 2 and 3 have some aspects that perhaps deserve to be published, but it is not clear to me how useful these are (not very much in my opinion). References to aircraft observations are vague and missing the key aspect, which is the irrelevance of an idealized problem considered by the authors to low-spatial resolution observations of a complicated multiscale natural system.

® The overview sections, which were copied and pasted for all three different reviews, can be summarized by the following claims:

a) The problem of turbulent mixing in clouds "seemed to be a popular topic some time ago", but now "the subject is old news".

b) This study addresses a "highly idealized problem" and uses simplified models in order to describe cloud mixing.

c) The results presented in the papers are not new and are “repeating already published material”.

The authors strongly disagree with the above statements of Referee 1.

In response to the first claim: the mechanism of mixing is still not well understood and continues to be a highly relevant problem in the cloud physics community, especially given the high rate of recent publications on this topic. We believe that the three papers contribute significantly to the theory of interaction of cloud droplets with turbulent environment and present novel techniques of investigating the effect of mixing both from a theoretical standpoint and through in-situ observations.

Second, in contrast to the reviewer, we support the common practice of using idealized models of complex cloud processes, in order to investigate physical mechanisms without being bogged down by the multitude of other processes involved. Idealized considerations (e.g. adiabatic assumptions) are widely used in cloud physics as well as in physics in general. The assumptions are clearly articulated at the beginning of each paper in order to let a reader judge about the level of idealization of the utilized approaches.

Third, as regards to novelty, the following new results have been obtained:

a) The first paper suggests a new technique for identifying type of mixing (homogeneous or inhomogeneous) based of the analysis of the moments of droplet size distributions. It was shown that homogeneous mixing breaks functional relationships between the moments. Nothing like that has been done before. A novel approach for identifying mixing from in-situ observations was proposed. The comments obtained by the authors from their colleagues showed that the proposed technique start to be utilized by other research groups.

b) The second paper considers *homogeneous* mixing. One of the important finding of this paper is an analytical universal solution describing the rate of evolution microphysical parameters as well as the final equilibrium state (mixing diagram). It is shown that in case of polydisperse droplet size distributions evolution of droplet spectra can lead to increase in characteristic size of droplets in contrast to widely accepted "classical" view, when the characteristic droplet size is decreasing. It was shown that evaporation time can be expressed in terms of time of phase relaxation. This is important for definition of reaction time in Damkoller number.

c) The third paper is dedicated to *inhomogeneous* mixing. A theoretical framework for a time dependent mixing of two volumes that accompanies by cloud droplet evaporation is developed. A new turbulence-evaporation model of time evolution of ensemble of droplets under different environmental parameters is proposed. In contrast to previous studies the Damkoller number is introduced as a result of re-normalization of mixing-evaporation equation, rather than empirically. It is shown that any mixing leads to droplet spectrum broadening. For

the first time the scientifically grounded demarcation between homogeneous and inhomogeneous mixing in the space of environmental parameters is performed.

The authors regret that Referee 1 overlooked all these novelties.

The authors also believe it is impossible to follow the recommendation of Referee 1, to combine all papers into one single, summary paper. While the papers all consider the same subject, they perform completely different functions with regard to investigating the issues of mixing.

General comment. Part 2 provides detailed analysis of the temporal evolution of the thermodynamic homogenization after the mechanical mixing quickly homogenizes the initially separated cloudy and cloud-free (i.e., sub-saturated) volumes. I feel Part 2 presents some relevant results, but the paper is way to long for the outcomes it provides. I hope my comments below will help the authors to convert this part into a section of the rewritten new manuscript.

(R) We appreciate this comment of Reviewer. However, we do not see the possibility to compress all parts of the study into one paper. The topics discussed in these parts as well as the approaches used are too different to combine them into one paper.

(C) 1. Towards the end of the introduction, the paper (once again) introduces the relevant time scales. What I find interesting and worth pursuing in my view is that the time scale describing droplet evaporation, taken as the phase relaxation time scale in the current study, is not the only possibility. Others (including the Jarecka et al. paper I think) have taken this time scale as the time required to evaporate a droplet with the sub-saturation of the cloud-free volume. I think some studies considered both and took the smaller (or the larger?) of the two (Feingold?). Note that the phase relaxation time scale has no information about the sub-saturation of the initially cloud-free volume, but the other definition does. Is this relevant? It should be for the extremely inhomogeneous mixing I think (I will comment on that in my review of Part 3).

(R) We know that some authors indeed use evaporation time of individual drop under given sub-saturation as a characteristic time of mixing process. In our opinion only phase relaxation time should be used as a characteristic time scale of the process since we should consider behavior of a large amount of droplets. In the paper (Pt 2) is shown that the phase relaxation time is a natural

time scale of mixing problem. This is clearly seen from universal renormalized evaporation equations, in which the phase relaxation time plays the role of time unit. Adiabatic consideration of the total volume in which mixing takes place leads to strict relationships between the changes of supersaturation (or sub-saturation) and liquid water content in the volume, that makes absolutely impossible to consider the changes in the size of individual droplet and in supersaturation independently. These two quantities (supersaturation and liquid water content) are tightly linked.

Note that supersaturation (or sub-saturation) is not in the list of parameters that determine phase relaxation time. Thus, the consideration of evaporation of individual droplet (under unchanged supersaturation) is not physically grounded and cannot be a time scale related to the mixing process. This comment is added to conclusion of Pt2.

2. Top of p. 30274. The Damkoehler number was introduced much earlier that Lehmann (2009), not using the name. Old paper by Latham, Baker and others should be cited here.

(R) Done

3. P. 30275. I think the fact that S can be taken as a linear combination of the supersaturations between the two volumes after the end of the mechanical mixing is an interesting observation. However, the small temperature difference assumption may be valid for the cumulus, but it is likely invalid for the subtropical stratocumulus. The inversion jump there is typically around 10K and the very top of the cloud may be exposed to several degree temperature differences between cloudy and cloud-free air.

(R) Very high temperature jumps like 10C above cloud top of stratocumulus cloud indicate, supposedly, the absence of intense turbulent mixing between cloud and dry air. In many cases temperature jumps is a few degrees C (H. Riehl). Penetration of clouds from BL to the inversion layer and their evaporation within this layer indicates the existence of strong interaction between Sc and the inversion layer.

A comment is included: At temperature differences of 5-10 ^{o}C, the deviation from the analytical solution (6) increases, which requires using more precise formulas for supersaturation (see Pt. 1).

4. Section 3 should be compressed. Section 3.1 shows formulas already introduced and used earlier in the paper (Part 1).

Formulas presented in Appendix A of Pt 1 which are the same as used in 3.1 of Pt 2 are deleted (since they are not used in Pt 1).

(C) Section 3.2 should be combined with 3.3 focusing on the key outcome (shown in Fig. 3). Section 3.3 provides a universal (i.e., using nondimensional parameters) analysis of the problem. As much as it is interesting, it is not very useful in my opinion. My suggestion is to compress it into an appendix in the rewritten paper.

(R) We disagree with Reviewer. We believe that obtaining of universal dependencies is one of the most important results of the study. This universal solution clearly shows the comparative role of different microphysical and thermodynamical parameters. This role is hardly possible to get from numerical studies. Note that Formula (6b) and Fig. 6b show actually the analytical expression for widely used mixing diagrams. Thus, we cannot shorten this section or move it to an appendix.

(C) The conclusion at the end of section 3.3 that the time scale is the phase relaxation time scale is trivial. Is the phase relaxation time scale about a response of the system to the supersaturation perturbation? The end of the mechanical mixing is exactly such a perturbation. So what is new here?

(R) As was mentioned in our response to Comment C1 of Reviewer, we wanted to stress that the phase relaxation time is a natural time scale of mixing problem in contrast to other time scales considered in literature.

(C) Figs. 3 and 4 and their discussion are not needed. Of course the time scale based on the initial radius changes as droplets evaporate and the mean radius decreases.

(R) Figs. 3 and 4 (and corresponding discussions) show:

a) time dependencies of microphysical characteristics during process of homogeneous evaporation under different initial parameters. Note that in standard mixing diagrams only final equilibrium states are considered. The figures show that the droplet relaxation time is the characteristic time scale.

b) the figures clearly demonstrate the existence of two different possible final regimes which depend in the initial relative humidity (or on universal non-dimensional parameter). These

regimes are: total droplet evaporation and termination of evaporation by reaching saturation state; curves separating these two regimes are also presented.
c) it is shown that the theory developed in the study agrees well with the numerical solution of more complicated non-linear equation for supersaturation.
Thus, these figures hardly can be excluded.

(C)5. Section 4 considers a polydisperse case. As before, I did not attempt to follow the derivations, but as I stated before I consider this problem trivial: you know how much water has to be left at the end (i.e., after the parcel is brought to saturation), so the only problem is how much shift of the spectrum is needed. I am not sure if obtaining detailed formulas for the evolution of various quantities is of significance in this highly idealized problem.

(R) This part illustrate non-trivial features of homogeneous mixing in case of initial polydisperse DSD. It is shown that (in contrast to general opinion)
a) Homogeneous mixing can be accompanied by a decrease in droplet concentration;
b) Homogeneous mixing may lead to an *increase* in the mean volume and an increase in the effective radii. The increase or decrease in the effective radii depend on the characteristic of initial DSD.

Since in real clouds DSDs are polydisperse, the widely accepted believes that homogeneous mixing always decreases effective radius keeping droplet concentration unchanged is wrong. These conclusions are main ones of the Pt2.

We would like to stress that consideration of such "highly idealized problem" showed results that were not recognized by investigators for many years. This study shows, therefore, that even such simplified model has direct relation to real clouds in which DSDs are polydisperse and time dependent.

6. Section 5 does not belong to this paper, not in this form. First, the authors talk about “parcels”. Which fluid flow model applies parcels in its formulation? I think the authors mean “grid volumes”, not “parcels”. Second, finite-difference fluid flow models (with some exceptions) typically assume that a grid volume is homogeneous. Any flux in and out (advection, turbulence, etc) leads in instantaneous homogenization of such a grid volume after completion of the time step. So obviously such a model does “homogeneous mixing”. This is trivial. One can design a

model (or scheme) that includes (i.e., assumes) a subgrid-scale structure of model-predicted variables, but this is a different story. Overall, section 5 is perhaps a start for a new scheme development, but it does not belong to this paper.

(R) This is not so trivial as reviewer assumes. The mixing that is simulated in any model is inhomogeneous at resolvable scales (the text is clarified) and typically homogeneous at the subgrid scale. Since we consider the understanding of this point is actual for cloud community, we decided to keep this section as Discussion, because it is important for cloud modelers.

7. Conclusion section is again short. As I said before, I consider point 2 a trivial consequence of the bulk evaporation in case when small droplets in the initial distribution have to evaporate completely.

(R) We suppose that if we would follow all recommendations of Reviewer concerning shortening and deleting entire sections, the conclusions would be indeed short. We believe, however, that in our responses we managed to show that results obtained are new and not trivial. As regards to specific comment of Reviewer to point 2 of conclusions, we agree that indeed the result is natural and easy to understand. The problem, however, is that during many years investigators believe (see, for example, comments of reviewer 2) that homogeneous mixing always decreases drop size, mean volume radius, but keeps droplet concentration constant. This is a wrong believe, because in contrast to the classical concept, the DSDs in real clouds are polydisperse.

Response to comments and remarks of reviewer 2

We are grateful to Reviewer for this high evaluation of the study

Comments on "Theoretical investigation of mixing in warm clouds – Part 2: Homogeneous mixing"

The significant contribution in this paper is the development of analytical results for the time evolution of a droplet size distribution for both monodisperse and polydisperse droplets in the limit of homogeneous mixing. The novelty in this, as far as I am aware, is that previous work has focused on the final stage of the distribution, such as commonly portrayed in the mixing diagram. Although it is idealized work, the non-dimensional equations and parameters in Equations 16 to 19 provide nice insight into cloud response to mixing. In particular, the finding that polydisperse droplet populations can show signatures typically interpreted as due to inhomogeneous mixing is insightful.

®We are grateful to Reviewer for this high evaluation of the study.

General criticisms:

©1. The introduction should provide better and clearer motivation for why a study of the time evolution of the droplet size distribution is of interest. This would be more valuable than additional discussion of general mixing concepts that already are covered in part 1.

® The introduction is improved and necessary comments are included.

©Also, as with part 1, the link between this paper and the other two parts needs to be clearly defined. What are the assumptions and limitations, and what is the area of application for the present work, especially relevant to the other two parts? With regards to the connection to other work, is Figure 1 in this part 2 really necessary, given that a similar version already is at the foundation of part 1 (part 1 Figure 1)?

® We did not introduce any additional assumptions as regards to homogeneous mixing. In contrast to typically used basic concept of homogeneous mixing we consider a) time evolution of droplet ensemble in a volume, where all droplets experience the same sub-saturation and b) we also consider the case when initial DSDs are polydisperse. Corresponding comment is added into

the introduction. We also increase the number of cross-references between different parts of the paper.

©Finally, it is absolutely necessary that the notation between the three papers should be uniform. This currently adds a lot of confusion in trying to understand the results of part 2 in the context of the results obtained in part 1.

® Notations are corrected and brought into line.

©2. Overall I would say that, while I view this as insightful work, there is a general need throughout the paper to discuss more about the physical interpretation rather than just writing down equations. For example, Eq. 23 is too complicated.

® Comments to eq. 23 are given

Specific comments

©1. S is supersaturation in Part 2 and 3, but it is saturation ratio in Part 1 and most textbooks. Choose one symbol and be consistent in all parts.

® The correction is made. S is supersaturation in all three parts

©2. Liquid water content and liquid water mixing ratio are different. In the text, q is liquid water mixing ratio, but the authors sometimes refer to it as LWC. For example, section 3.2 “Time evolution of supersaturation and LWC”, section 4.3 “Evolution of LWC and supersaturation”. The authors need to check the whole text and make it consistent.

® Corrected. Note we prefer to write down formulas using liquid water mixing ratio (kg/kg), but in the figures we show LWC (g/m^3). This is why we use word LWC in the names of sections

©3. Page 30279, line 14: missing space between “parameter” and “gamma”.

® corrected

©4. Equation 22 on page 30280: should have a “~” over “t” for “S(t)”.

® corrected

5. Page 30288, line 20-22: I don't understand "the concept of homogeneous mixing, according to which the mean and effective radii do not change." Please clarify.

® The sentence is corrected. An increase in the value of the effective radius contradicts the concept of homogeneous mixing, according to which both the mean radii and the effective radii decrease in the course of mixing.

©6. Appendix B: Equation number in the text (for example page 30298 Line 15) should be "BX" not "AX"

® Corrected

©7. Figure 3 caption: should be "LWC=0.29g/m3" not q

® Corrected

©8. Figure 6b: should be normalized liquid water mixing ratio not LWC

® Corrected

©9. Figure 7a: x axis should be 0, 5 10 15?

® Corrected

©10.Figure 7 caption: also q should be LWC.

® Corrected

Theoretical investigation of mixing in warm clouds. Part 2: Homogeneous mixing

M. Pinsky(1), A. Khain(1), A. Korolev(2) and L. Magaritz-Ronen (1)

(1) Department of Atmospheric Sciences, The Hebrew University of Jerusalem, Israel

(2) Environment Canada, Cloud Physics and Severe Weather Section, Toronto, Canada

Submitted to the Atmos. Chem. Phys.

revision (April, 2016)

Communicating author: Alexander Khain, The Hebrew University of Jerusalem,

alexander.khain@mail.huji.ac.il

Abstract

Evolution of monodisperse and polydisperse droplet size distributions (DSD) during homogeneous mixing is analyzed. Time-dependent universal analytical expressions for supersaturation and liquid water content are derived. For an initial monodisperse DSD, these quantities are shown to depend on a sole non-dimensional parameter. The evolution of moments and moment-related functions in the course of homogeneous evaporation of polydisperse DSD is analyzed using a parcel model.

It is shown that the classic conceptual scheme, according to which homogeneous mixing leads to a decrease in droplet mass at constant droplet concentration, is valid only in cases of monodisperse or initially very narrow polydisperse DSD. In cases of wide polydisperse DSD, mixing and successive evaporation lead to a decrease of both mass and concentration, so the characteristic droplet sizes remain nearly constant. As this feature is typically associated with inhomogeneous mixing, we conclude that in cases of an initially wide DSD at cloud top, homogeneous mixing is nearly indistinguishable from inhomogeneous mixing.

Key words: *turbulent mixing, homogeneous mixing, mono-and polydisperse droplet size distributions*

1. Introduction

Turbulent mixing at cloud edges and cloud tops accompanied by phase transitions has been the focus of numerous studies, beginning with the pioneering works of Baker and Latham (1979), Baker et al. (1980), Blyth et al. (1980) and Baker and Latham (1982). Laboratory experiments by Latham and Reed (1977) showed that after mixing with sub-saturated air some droplets completely evaporate while others remain unchanged. This finding gave rise to the concept of two types of turbulent mixing: homogeneous and inhomogeneous. A recent description of the classical concepts of homogeneous and inhomogeneous mixing can be found in study by Korolev et al. (2016), hereafter referred to as Pt1.

Figure 1 presents a conceptual scheme of homogeneous mixing between saturated cloud volume V_1 containing droplets and sub-saturated droplet-free volume V_2 (Fig. 1a) in case of initially monodisperse droplet size distribution (DSD). This scheme is the base of further analysis. According to the concept of homogeneous mixing, the air within the volumes mixes at a rate much higher than the characteristic rate of droplet evaporation. So, the fields of temperature and humidity (and, therefore, the fields of the relative humidity and supersaturation) are rapidly homogenized throughout the entire volume, and all the droplets experience the same supersaturation (Fig. 1b). At the end of the first stage, the droplet concentration decreases due to dilution down to $N_{m0} = N_1 \frac{V_1}{V_1 + V_2}$, where N_1 is the initial droplet concentration in the cloud volume. At the second stage (Fig. 1c), droplets change supersaturation and temperature through their evaporation. There are two possible scenarios for the final equilibrium states. In the first one, illustrated in Fig. 1c, droplets continue evaporating until they saturate the environment. The size of all droplets decreases, but they evaporate only partially, so the droplet concentration N_{m0} remains unchanged. In the second scenario, when the initially droplet-free volume is very dry,

357 the droplets penetrated from cloud volume evaporate completely. In case of polydisperse initial
358 DSD, both partial and complete evaporation of droplets determine the final DSD.

359 In contrast to homogeneous mixing, spatial homogenization during *inhomogeneous* mixing is
360 a relatively slow process. According to the concept of extremely inhomogeneous mixing, some
361 droplets are transported by the turbulent eddies into the dry environment and experience
362 complete evaporation, whereas other droplets remain unchanged. As in the case of homogeneous
363 mixing, the process of droplet evaporation continues until either the environment is saturated or
364 all the droplets evaporate. According to the classical concept, during extremely inhomogeneous
365 mixing the shape of DSD is conserved, however, the total droplet concentration decreases (see
366 review by Devenish et al., 2012 and Pt 1).

367 The classical concepts analyze only the final equilibrium states which are based on the mass
368 conservation consideration. Strictly speaking, the size distributions in the final states, assumed in
369 the classical concepts, are hypothetical and cannot be reached. This is because the classic
370 concepts do not take into account the mixing-induced DSD broadening. Detailed simulation of
371 time evolution of DSD and other microphysical parameters is necessary not only to better
372 determine the final states, but also to evaluate time periods during which such final states are
373 reached. The analysis of time evolution is practically important because many DSDs measured
374 in-situ correspond to the transient state, but not to the final equilibrium state. Besides, it is
375 necessary to determine the evolution of initially polydisperse DSD, that may substantially differ
376 from the evolution of monodisperse DSD.

377 We analyze the time evolution of the DSD during homogeneous mixing in cases of
378 monodisperse and polydisperse initial DSDs. The analysis is based on new equations and
379 methodology developed by Pinsky et al. (2013, 2014).

380 First, we need to evaluate conditions at which mixing can be considered homogeneous. The
381 characteristic spatial scale of homogeneous mixing can be estimated by comparing the

382 characteristic times of two processes providing thermodynamic equilibrium inside a mixing
383 volume. The first process is mechanical mixing (diffusion) governed by turbulence. Turbulent
384 mixing leads to homogenization of temperature, humidity (and, thus, of supersaturation) as well
385 as of droplet concentration within the volume $V = V_1 + V_2$. The second process is evaporation of a
386 droplet ensemble, which leads to an increase in relative humidity and to the thermodynamical
387 equilibrium in the mixing volume.

388 The process of mixing that is accompanied by droplet evaporation is characterized by two
389 time scales. The first time scale is the characteristic mixing (homogenization) time τ_{mix} of an
390 entrained volume with linear scale L_{mix} can be evaluated from the relationship (Monin and
391 Yaglom, 1975)

392 $$\tau_{mix} = \varepsilon^{-1/3} L_{mix}^{2/3} \quad , \qquad (1)$$

393 where ε is the turbulent kinetic energy dissipation rate. The estimation (1) suggests that the size
394 of the volume falls within the inertial interval of turbulence. Therefore, after the time τ_{mix},
395 volume with a linear scale of about L_{mix} will be mechanically homogenized and all the droplets
396 in the volume will experience the same supersaturation.

397 The second time scale characterizes rate of droplet evaporation and corresponding changes of
398 supersaturation. In this study, as well as later in Part.3, it will be shown that the characteristic
399 evaporation time is the *phase relaxation time* τ_{pr}, that determines the rate of change of
400 supersaturation during condensation or evaporation (Mazin, 1968; Korolev and Mazin, 2003)

401 $$\tau_{pr} = \left(4\pi \mathscr{D} \bar{r} N\right)^{-1}, \qquad (2)$$

402 where $N = N_{m0}$ is the concentration of droplets in the mixing volume, $\bar{r}$ is the mean radius of
403 droplets and $\mathscr{D}$ is the diffusivity of water vapor. The spatial scale at which the mixing time is

404 equal to the phase relaxation time is called a phase relaxation scale L_{pr} (Mazin, 1968). This scale
405 can be calculated from Eqs. (1) and (2) as

406 $$L_{pr} = \varepsilon^{1/2}\tau_{pr}^{3/2} \approx \varepsilon^{1/2}\left(4\pi\mathscr{D}\bar{r}N\right)^{-3/2} \quad (3)$$

407 The type of mixing is often characterized by the value of the Damköhler number which in
408 regard to atmospheric mixing is defined as the ratio τ_{mix}/τ_{pr} (Baker et al., 1980; Jeffery, 2007;
409 Lehmann et al., 2009):
410
411 $$Da = \frac{\tau_{mix}}{\tau_{pr}} = \frac{4\pi\mathscr{D}\bar{r}NL_{mix}^{2/3}}{\varepsilon^{1/3}} \quad (4)$$

412 The case $Da << 1$ corresponds to homogeneous mixing, when mechanical homogenization
413 occurs much faster than does droplet evaporation. The case $Da >> 1$ corresponds to extremely
414 inhomogeneous mixing. It is reasonable to consider the value $Da = 1$ as a boundary separating
415 the two types of mixing. This condition is equivalent to the condition
416
417 $$L_{mix} = L_{pr} \approx \varepsilon^{1/2}\left(4\pi\mathscr{D}\bar{r}N\right)^{-3/2} \quad (5)$$

418
419 Expression (5) determines the maximum spatial scale at which mixing can be considered as
420 homogeneous. The evaluation of the spatial scales at conditions typical of different cloud types
421 is presented in **Table 1**. One can see that the characteristic volume size at which mixing can be
422 considered homogeneous ranges from 0.2 m to 0.6 m. At larger scales, supersaturation within the
423 mixing volume is non-uniform and droplets in the volume experience different values of relative
424 humidity. In this case, the mixing should be considered inhomogeneous.
425 The further paper structure is the following. In Section 2 we calculate the thermodynamic
426 characteristics of the resulting volume at the end of the first stage of mixing (see Fig. 1b).

427 Section 3 presents an analytic solution of homogeneous droplet evaporation in the monodisperse
428 DSD case. In Section 4 effects of polydispersivity on the DSD evolution are described. The
429 problem of turbulent mixing representation in numerical cloud models is discussed in Section 5.
430 The main results of the study are presented in Conclusion Section 6.
431

432 **2. Thermodynamic characteristics of the mixing volume at the end of the first stage**

433 At the first stage (see the scheme in Fig.1) homogeneous mixing is considered as an isobaric
434 process that is not accompanied by phase transitions (Korolev and Isaac, 2000). Let us consider
435 mixing between a cloud volume with mass m_1, supersaturation $S_1 = 0$ and temperature T_1 and a
436 droplet-free volume with mass m_2, supersaturation $S_2 < 0$ and temperature T_2. The cloud
437 volume also contains droplets with concentration N_1 and liquid water mixing ratio q_1 (Fig. 1).
438 For the sake of simplicity, we assume that the mass of both volumes is equal to one. Let us
439 further assume that μ is the mass fraction of the cloud air that mixes with the mass fraction
440 $(1-\mu)$ of the droplet-free air. In this case, the air mass in the mixing volume will be equal to
441 $m_1\mu + (1-\mu)m_2 = 1$. Isobaric mixing leads to an approximate linear dependence of droplet
442 concentration N_{m0} on μ.

443 After an instantaneous homogenization of the two volumes, the intermediate temperature
444 T_{m0}, droplet concentration N_{m0} and liquid mixing ratio q_{m0} are (see Pt.1):

445 $$N_{m0} = N_1\mu; \quad q_{m0} = q_1\mu; \quad T_0 = T_1\mu + T_2(1-\mu) \qquad (6a)$$

446 If the temperature difference $|T_1 - T_2|$ does not exceed a few degrees, the intermediate
447 supersaturation S_{m0} can be approximated by a linear dependence on μ

448 $$S_{m0} = S_2(1-\mu) \qquad (6b)$$

449 **Figure 2** shows, that in case $|T_1 - T_2| < 2^{o}C$, the deviations of supersaturation from the linear
450 dependence (6b) are small enough and can be neglected. In cases when the temperature of the
451 dry volume substantially differs from the temperature of the cloud volume, the dependence of the
452 resulting supersaturation on parameter μ becomes non-linear (Fig. 2). At temperature
453 differences of 5-10 ^{o}C, the deviation from the analytical solution (6) increases, which requires
454 using more precise formulas for supersaturation (see Pt. 1). Values of N_{m0}, q_{m0}, T_{m0} and S_{m0}
455 determine the initial conditions for the second stage of homogeneous mixing. This is actually
456 homogeneous evaporation of droplets, which leads to a thermodynamic equilibrium between
457 water vapor and liquid water.
458
459 **3. Analysis of homogeneous droplet evaporation in the monodisperse DSD case**
460
461 **3.1. Basic assumptions and equations**
462 The second stage of mixing consists in homogeneous evaporation of droplets. The evolution
463 of DSD during the second stage is considered here under the following assumptions: a) the
464 processes inside the mixing volume are adiabatic, b) the droplet size distribution is
465 monodisperse, c) the vertical velocity of the volume $u_z = 0$ and d) the sedimentation of droplets
466 is neglected and their concentration remains constant.
467 The liquid water mixing ratio can be expressed as
468 $$q(t) = \frac{4\pi\rho_w}{3\rho_a} N r^3(t) \qquad (7)$$
469
470 where $r(t)$ is the radius of droplets and N is the droplet number concentration. Closed
471 equations describing condensation/evaporation in a moving adiabatic air volume were obtained

by Pinsky et al. (2013). In an unmoving adiabatic volume, evaporation is described by the equation for supersaturation (e.g., Korolev and Mazin, 2003)

$$\frac{1}{S+1}\frac{dS}{dt} = -A_2\frac{dq}{dt} \tag{8}$$

and droplet evaporation is described by the simplified equation (Pruppacher and Klett, 2007)

$$r\frac{dr}{dt} = \frac{S}{F}, \tag{9}$$

where S is the supersaturation over a flat water surface. For cloud droplets Eq. (9) is valid with high accuracy. We do take into account formation of haze particles resulting from droplet evaporation. This allows us to neglect the curvature term and chemical term in the evaporation equation. Coefficients A_2 and F in Eqs. (8, 9) are slightly dependent on the temperature and the pressure

$$A_2 = \frac{1}{q_v} + \frac{L^2}{c_p R_v T^2} \tag{10}$$

$$F = \frac{\rho_w L^2}{k_a R_v T^2} + \frac{\rho_w R_v T}{e_S(T)\mathscr{D}} \tag{11}$$

We assume that coefficients A_2 and F do not change in the course of droplet evaporation.

The physical meaning and units of other variables are given in **Appendix A.**

3.2. Time evolution of supersaturation and of liquid water content

The closed differential equations for the liquid water mixing ratio q and supersaturation S to be used in the analysis are derived in **Appendix B.**

$$\frac{dq}{dt} = BN_{m0}^{2/3}\left[(S_{m0}+1)\exp\{-A_2(q-q_{m0})\}-1\right]q^{1/3} \tag{12}$$

$$\frac{1}{S+1}\frac{dS}{dt} = -A_2 BN_{m0}^{2/3} S\left(q_{m0} - \frac{1}{A_2}\ln\frac{S+1}{S_{m0}+1}\right)^{1/3} \tag{13}$$

where

$$B = \frac{3}{F}\left(\frac{4\pi\rho_w}{3\rho_a}\right)^{2/3} = const \qquad (14)$$

The solutions of these equations depend on the values of N_{m0}, q_{m0}, T_{m0}, and S_{m0}, obtained after the first stage of mixing. Eqs. (12) and (13) are rigidly connected by the following equation directly following from Eq. (8):

$$\ln[S(t)+1] = -A_2 q(t) + C \qquad (15)$$

where $C = \ln[S_{m0}+1] + A_2 q_{m0}$ is determined by the initial conditions at $t = 0$.

Since in this study we assume $S(t) \le 0$, it is convenient to use the relative humidity RH and the saturation deficit SD to characterize the thermodynamic state of the mixing volume. Both quantities are easily related to $S(t)$: $SD(t) = -S(t)$, $RH(t) = 1 + S(t)$. **Figure 3** demonstrates dependencies $S(t)$ and $q(t)$, calculated at an initial relative humidity RH_{m0} that varies from 72% to 91.6%, and an initial LWC of 0.6 gm^{-3}. RH_{m0} corresponds to the relative humidity in dry volume RH_2, that ranges from 43% to 83% at $\mu = 0.5$. The results of solving Eqs. (14-15) were compared with those obtained using a parcel model (Korolev, 1995) in which evaporation is described using equations with temperature-dependent parameters, and were found to be in excellent agreement. This agreement can be attributed to the fact that temperature changes that occurred in the course of the mixing are relatively small, validating the assumption about the constancy of A_2 and F.

As seen from Fig. 3, the final equilibrium state may be reached within several seconds. Fig. 3 shows the possibility of the two final states mentioned above: a) complete droplet evaporation

reached at different time instances depending on the initial value of S_{m0}, and b) partial droplet evaporation at $RH_{m0} > 82\%$. In the latter case, the final supersaturation is equal to zero.

3.3. Universal dependencies of supersaturation and of LWC on time

In order to simplify the further analysis we introduce the following non-dimensional parameters: normalized liquid water mixing ratio $\tilde{q} = \frac{q}{q_{m0}}$ which is equal to normalized liquid water content, normalized supersaturation $\tilde{S} = \frac{S}{A_2 q_{m0}}$, and non-dimensional time $t = t/\tau_{m0}$, where $\tau_{m0} = \left(BA_2 N_{m0}^{2/3} q_{m0}^{1/3}\right)^{-1}$ is the time scale. Then the set of non-dimensional equations describing changes of supersaturation and liquid mixing ratio can be written as (see Appendix B for detail)

$$\tilde{S}(\tilde{t}) = -\tilde{q}(\tilde{t}) + \gamma \qquad (16)$$

$$\frac{d\tilde{q}}{d\tilde{t}} = \tilde{q}^{1/3}\left(\gamma - \tilde{q}\right) \qquad (17)$$

$$\frac{d\tilde{S}}{d\tilde{t}} = -(\gamma - \tilde{S})^{1/3}\tilde{S}, \qquad (18)$$

where

$$\gamma = 1 + \frac{S_{m0}}{A_2 q_{m0}} = 1 + \frac{1-\mu}{\mu}\frac{S_2}{A_2 q_1} \qquad (19)$$

is dimensionless parameter which depends on the initial supersaturation S_{m0} and the initial liquid water mixing ratio q_{m0}. The value of this parameter can be either positive or negative. Eqs. (16-18) are strictly valid if $|S_{m0}| << 1$, i.e. when the value of supersaturation S is negligible in comparison with unity in the factor $(S+1)^{-1}$ on the left-hand side of Eq. (8). However, a detailed comparison of solutions of Eqs. (16-18) with those obtained using a numerical model showed

that Eqs. (16-18) provide accurate solution at RH_{m0} as low as 30-40%. Eq. (17) should be solved with the initial condition $\tilde{q}(0)=1$, and Eq. (18) should be solved with the initial condition $\tilde{S}(0)=\frac{S_{m0}}{A_2 q_{m0}}<0$. Therefore, solutions of both equations depend on the sole parameter γ. Eqs. (17) and (18) are rigidly connected by balance equation Eq. (16).

Defining $x(\tilde{t})=\left(\tilde{q}(\tilde{t})\right)^{1/3}$ and $\chi=|\gamma|^{1/3}\mathrm{sgn}(\gamma)$, the solution of Eq. (17) with the initial condition $x(0)=1$ is

$$2\chi\tilde{t}=\ln\left[\frac{(1-\chi)^2}{(x-\chi)^2}\frac{x^2+\chi x+\chi^2}{1+\chi+\chi^2}\right]+2\sqrt{3}\left[\mathrm{atan}\frac{2\sqrt{3}\chi(1-x)}{3\chi^2+(2+\chi)(2x+\chi)}\right] \qquad (20)$$

The solution for the normalized supersaturation can be obtained from Eq. (20) and the balance equation (16)

$$\tilde{S}(\tilde{t})=-\tilde{q}(\tilde{t})+\gamma=-x^3(\tilde{t})+\chi^3 \qquad (21)$$

Figure 4 demonstrates time dependencies $\tilde{S}(\tilde{t})$ and $\tilde{q}(\tilde{t})$ calculated at different γ at $S_{m0}>-10\%$ (i.e. $RH_{m0}>90\%$). As seen from Fig. 4. the analytical solution is quite close to the numerical one. The deviation increases with an increase in parameter γ. At $\gamma=-0.5$, the error in the final *RH* is about 15%. The initial RH_{m0} in this case is about 90 %. RH_{m0} is the relative humidity in the mixing volume V after the first stage of mixing. As mentioned above, RH_{m0} may be substantially higher than RH_2 in the initially droplet-free volume. *In-situ* measurements (Gerber et al., 2008) and remote measurements of aerosol humidification (Knight and Miller, 1998; Bar-Or et al., 2012) indicate the existence of zones of high *RH* along cloud edges. These observations and results of numerical simulations indicate that the analytical solution (20-21) is a universal one and applicable at any RH values in cloud surrounding.

554 The amplitude of the deviation of the analytical solution for supersaturation from the
555 modeled result decreases with the decrease of γ. The cause of the deviation is neglecting term
556 $(S+1)$ on the left-hand side of Eq. (8).

557 There are two types of solutions determined by parameter χ (or parameter γ), separated by
558 value $\chi = 0$ (Figs. 3 and 4). Condition $\chi = 0$ corresponds to $\mu = \mu_{cr}$ (see Pt 1) and indicates
559 complete evaporation of all the droplets and the relative humidity increasing up to 100 %.
560 Condition $\chi > 0$ corresponds to solutions $\tilde{q}(\tilde{t})$ with asymptotic behavior at $\tilde{t} \to \infty$: $\tilde{q} \to \gamma$ and
561 $\tilde{S} \to 0$, which means that droplets do not completely evaporate. Condition $\chi < 0$ means that all
562 the droplets completely evaporate.

563 At $\chi = 0$, the analytical solution is:

564 $$x = \frac{3}{\tilde{t}+3}; \quad \tilde{q}(\tilde{t}) = \left(\frac{3}{\tilde{t}+3}\right)^3; \quad \tilde{S}(\tilde{t}) = -\left(\frac{3}{\tilde{t}+3}\right)^3 \qquad (22)$$

565 Both LWC and supersaturation tend to zero at $\tilde{t} \to \infty$.

566 At $\chi < 0$, the duration of the evaporation is limited in time (Figs. 3, 4). Normalized
567 evaporation time t_e depends on parameter χ only. This dependence can be obtained from Eq.
568 (20) at $x = 0$:

569 $$t_e = \frac{1}{2\chi} \ln \frac{(1-\chi)^2}{1+\chi+\chi^2} + \frac{\sqrt{3}}{\chi} \operatorname{atan} \frac{\sqrt{3}}{2\chi+1} \qquad (23)$$

570 Here the time is counted in the relaxation time scales. This fact indicates that the phase
571 relaxation time is the time scale that should be used in the analysis of mixing. The choice of a
572 time scale will be discussed elaborated in greater detail below.

573 At $\chi > -1/2$, one have to use the values $\text{atan}\left(\frac{\sqrt{3}}{2\chi+1}\right)-\pi$ in Eq. (23) instead of $\text{atan}\frac{\sqrt{3}}{2\chi+1}$.

574 t_e is the time needed for supersaturation to reach its maximal value (Figs. 3a, 4a). This value is
575 calculated from Eqs. (16) and (6)

576 $$\tilde{S}_{\max} = \gamma = \chi^3 = 1 + \frac{S_{m0}}{A_2 q_{m0}} \approx 1 + \frac{S_2}{A_2 q_1}\frac{1-\mu}{\mu} = 1 + R\frac{1-\mu}{\mu} \qquad (24)$$

577 where $R = \frac{S_2}{A_2 q_1}$ is a dimensionless parameter describing the ratio of S_2 in the initially dry air
578 and the reserve of liquid water available for evaporation. (This parameter can be determined
579 more precisely using Eq. (2) or Eq. (4) given in Pt. 1).

580 The dependence $t_e(\chi)$ is shown in **Figure 5. O**ne can see that at large sub-saturation values
581 ($\chi < -0.4$) all the droplets evaporate within the span of a few relaxation times, and the analytical
582 results agree well with the model (benchmark) results. At a high initial *RH*, droplet evaporation
583 increases the humidity to nearly the saturation value, at which evaporation becomes extremely
584 slow. In this case, simplified analytical formulas overestimate the evaporation time.

585 At $\chi > 0$, droplets partially evaporate, q reaches the minimal value and the thermodynamic
586 equilibrium is reached when $S \to 0$. Minimal normalized equilibrium LWC can be found from
587 Eqs. (21) and (6)

588 $$\tilde{q}_{\min} = \gamma = \chi^3 = 1 + R\frac{1-\mu}{\mu} \qquad (25)$$

589 Eq. (25) is similar to Eqs. (4-5) (see Pt.1.).

590 Dependences of $\tilde{S}_{\max}$ and $\tilde{q}_{\min}$ on cloud air fraction, calculated at different initial conditions
591 using Eqs. (24) and (25) are shown in **Figure 6**. The diagram in Fig. 6b is actually a kind of
592 widely used mixing diagram for homogeneous mixing, and Eq. (25) is an universal analytic
593 equation for calculation of this diagram depending on the non-dimensional parameter R. Panel

(a) shows that the higher the cloud fraction of air parcels involved in mixing, the lower the saturation deficit, i.e. the higher the final *RH* is. At small R, saturation is reached at a low μ. Similar diagrams in physical units are shown in Pt.1 in Figs. 4a,g.

The equations presented above allow to predict the results of homogeneous mixing both for partial and complete evaporation of droplets (**Table 2)**. One can see that at low temperatures, the environment air volume becomes cloudy at relatively low values of liquid water content in the cloud volume even if *RH* of the environment volume is as low as 50%. The reason is that the saturation ratio at low temperatures is low and only a small amount of liquid should be evaporated to make the initially dry volume saturated.

The diagram in Fig.6b allows to calculate the final liquid water content remaining in the entire volume after saturation reaches 100%. This diagram also shows that for each value of μ there is a certain value of R at which full evaporation takes place. The remaining $\tilde{q}_{\min}$ increases with decreasing μ and increasing R, as shown by the arrow.

The natural time scale of the evaporation and, therefore, homogeneous mixing was determined as $\tau_{m0} = \left(BA_2 N_{m0}^{\ 2/3} q_{m0}^{1/3}\right)^{-1}$. This value is inversely proportional to $N_{m0} r_{m0}$ and actually coincides with the initial phase relaxation time τ_{pr}. The equality of the characteristic time scales of variations in supersaturation and in liquid water content directly follows from the equation (15). Indeed, in case of $|S| << 1$ the equation can be rewritten as $S(t) = -A_2 q(t) + C$ thus establishing a linear relationship between the supersaturation and the liquid water mixing ratio.

It should be emphasized that τ_{m0} is not the time of total droplet evaporation or the time of reaching saturation (when evaporation is over). The time of complete evaporation of all droplets can be substantially longer than phase relaxation time τ_{m0}.

4. Analysis of homogeneous droplet evaporation in case of a polydisperse DSD

618 **4.1. DSD evolution in the course of droplet evaporation**

619 To analyse polydisperse DSD evolution during droplet evaporation at the second stage of
620 homogeneous mixing, we use the same equations for diffusional growth (9) and supersaturation
621 (8) as those used in case of a monodisperse DSD. The solution of Eq. (9) can be written in the
622 form

623 $$r^2(t) = r_0^2 - Q(t) \tag{26}$$

624 where the non-negative function $Q(t) \geq 0$ is proportional to the supersaturation integral

625 $$Q(t) = -\frac{2}{F}\int_0^t S(t')dt' \geq 0 \tag{27}$$

626 This function characterizes a decrease in the square of droplet radii. At $t = 0$, $Q(0) = 0$. Let
627 $f_0(r_0)$ be an initial DSD immediately following the first stage of homogeneous mixing. This
628 distribution obeys the normalization condition

629 $$N_{m0} = \int_0^\infty f_0(r_0)dr_0 \tag{28}$$

630 where N_{m0} is the initial droplet number concentration after the first stage of mixing. Using the
631 inverse transformation $r_0 = \sqrt{r^2 + Q(t)}$ alongside with condition $r \geq 0$ and the relation between
632 the distribution functions $f(r,t) = f_0(r_0)\frac{dr_0}{dr}$ we get

633 $$f(r,t) = \begin{cases} \dfrac{r}{\sqrt{r^2 + Q(t)}} f_0\left(\sqrt{r^2 + Q(t)}\right), & r \geq 0 \\ 0, & r < 0 \end{cases} \tag{29}$$

634 Eq. (29) shows that the time changes in DSD and in its moments depend both on the initial DSD
635 at $t = 0$, $f_0(r_0)$ and on the time-dependent function $Q(t) \geq 0$.

636 To illustrate the DSD evolution using Eq. (29), we assume that the initial distribution
637 immediately following the first stage of mixing can be represented by a Gamma distribution:

638 $$f_0(r_0) = \frac{N_{m0}}{\Gamma(\alpha)\beta}\left(\frac{r_0}{\beta}\right)^{\alpha-1}\exp\left(-\frac{r_0}{\beta}\right) \quad (30)$$

639 where N_{m0} is an intercept parameter, α is a shape parameter and β is a slope parameter of
640 distribution. Different sets of parameters allow approximations of both narrow and wide DSD.
641 The parameters of the initial Gamma distribution used in this study are presented in **Table 3** and
642 are chosen so that the modal radii of DSD and the LWC would be the same for both
643 distributions.

644 Combining Eqs. (29) and (30) yields an equation for DSD evolution as a function of $Q(t)$

645 $$f(r,t) = \begin{cases} \dfrac{N_{m0}}{\Gamma(\alpha)\beta^{\alpha}}(r^2+Q)^{\frac{\alpha}{2}-1} r \exp\left(-\dfrac{\sqrt{r^2+Q}}{\beta}\right), & r \geq 0 \\ 0, & r < 0 \end{cases} \quad (31)$$

646 This DSD (31) depends on four parameters, wherein parameter $Q(t)$ increases with time
647 according to Eq. (27). Examples of evolutions of an initially narrow DSD and an initially wide
648 DSD are shown in **Figure 7**. All the calculations were performed using a parcel model (Korolev,
649 1995).

650 There is a significant difference between evolution of DSDs in cases of monodisperse and
651 polydisperse DSDs. At a monodisperse DSD, droplet concentration remains unchanged until the
652 final stage of evaporation when droplets become small and then all evaporate rapidly. At a
653 polydisperse DSD the droplet concentration decreases simultaneously with the decrease in
654 LWC. Evaporation of a the narrow size distribution is consistent with the concept of
655 homogeneous mixing (Fig. 7a). However homogeneous evaporation of droplets with a wide
656 DSD may be mistakenly taken for inhomogeneous mixing.

657

658 **4.2. Evolution of DSD moments and related functions**

Eq. (29) also allows evaluation of droplet concentration, DSD moments and related functions. Droplet concentration corresponds to the zero moment of DSD and can be expressed as

$$N(t)=\int_0^\infty f(r,t)dr=\int_0^\infty \frac{r}{\sqrt{r^2+Q(t)}}\,f_0\left(\sqrt{r^2+Q(t)}\right)dr=\int_{\sqrt{Q(t)}}^\infty f_0(r_0)dr_0 \qquad (32)$$

Since function $Q(t)$ monotonically increases with the time, the right-hand integral in Eq. (32) decreases, indicating a decrease in droplet concentration with time. If the initial distribution of droplets is described by a Gamma distribution, the decrease of droplet concentration with the time is evaluated using Eqs. (30) and (32) as

$$N(t)=\int_{\sqrt{Q(t)}}^\infty f_0(r_0,t)dr_0=\int_{\sqrt{Q(t)}}^\infty \frac{N_{m0}}{\Gamma(\alpha)\beta}\left(\frac{r_0}{\beta}\right)^{\alpha-1}\exp\left(-\frac{r_0}{\beta}\right)dr_0=$$

$$\frac{N_{m0}}{\Gamma(\alpha)}\int_{\frac{\sqrt{Q(t)}}{\beta}}^\infty x^{\alpha-1}\exp(-x)dx=N_{m0}\frac{\Gamma(\alpha,\eta)}{\Gamma(\alpha)}. \qquad (33)$$

where

$$\eta(t)=\frac{\sqrt{Q(t)}}{\beta} \qquad (34)$$

is a non-dimensional function of time and $\Gamma(\alpha,\eta(t))$ is an upper incomplete Gamma function (Korn and Korn, 2000). It follows from Eqs. (32) and (33) that $N(t)\le N_0$. The dependencies of the normalized droplet concentration $\frac{N(t)}{N_{m0}}$ on time for an initially narrow DSD and an initially wide DSD are shown in **Figure 8**.

Fig. 8 shows that in case of an initially narrow DSD, droplet concentration does not change during the first 20 s when $RH_{m0}=91.6\ \%$ because the DSD does not shift strongly enough toward smaller droplet radii. At lower initial supersaturations, droplet concentration decreases

679 with time. This decrease may take place rapidly and may last several seconds only. The red line
680 separates two different evaporation scenarios. The curves above the red line correspond to partial
681 evaporation and reaching the saturation state, whereas the curves below the red line correspond
682 to complete evaporation of droplets and the environment remains subsaturated.

683 At an initially wide DSD, droplet concentration decreases at any initial subsaturation value
684 because the DSD contains small droplets that start evaporating regardless the subsaturation
685 value. In the particular example shown in Fig. 8, the droplet relaxation time is shorter in case of a
686 wide DSD, so droplet concentration decreases slower than at a narrow DSD. Droplet
687 concentration decreases substantially during a few tens of seconds, but does not reach zero due
688 to a significant concentration of large droplets in the wide DSD. The equilibrium state is not
689 reached within 20 s.

690 Fig. 8 also demonstrates an excellent agreement between the results of analytical calculations
691 performed using Eq. (33) and results obtained using the parcel model.

692 A normalized moment of the *k-th* order is evaluated as

693 $$\overline{r^k(t)} = \frac{1}{N(t)}\int_0^\infty r^k f(r,t)dr = \frac{1}{N(t)}\int_0^\infty \frac{r^{k+1}}{\sqrt{r^2+Q(t)}} f_0\left(\sqrt{r^2+Q(t)}\right)dr = \frac{1}{N(t)}\int_{\sqrt{Q(t)}}^\infty \left(r_0^2 - Q(t)\right)^{k/2} f_0(r_0)dr_0$$

694

695 $$\overline{r^k(t)} = \frac{\int_{\sqrt{Q(t)}}^\infty \left(r_0^2 - Q(t)\right)^{k/2} f_0(r_0)dr_0}{\int_{\sqrt{Q(t)}}^\infty f_0(r_0)dr_0} \qquad (35)$$

696 In case when the initial distribution is given by the Gamma distribution (30), Eq. (35) leads to
697 the following equation

698 $$\overline{r^k}(t) = \frac{\beta^k}{\Gamma\left(\alpha,\eta(t)\right)}\int_{\eta(t)}^\infty \left(x^2-\eta^2(t)\right)^{k/2}\left(x\right)^{\alpha-1}\exp\left(-x\right)dx \qquad (36)$$

699 The even moments can be represented using incomplete the Gamma functions.

700 **Figures 9 and 10** show the time dependencies of quantities typically used for characterizing

701 the DSD shape, namely the mean radius $\bar{r}(t)$ (panel (a)), the effective radius $r_{eff}(t) = \frac{\overline{r^3}(t)}{\overline{r^2}(t)}$

702 (panel (b)), the RMS width of DSD $\sigma(t) = \sqrt{\overline{r^2}(t) - \bar{r}^2(t)}$ (panel (c)) and the dispersion

703 coefficient $\delta(t) = \frac{\sigma(t)}{\bar{r}(t)}$ (panel (d)). The dependencies corresponding to an initially narrow DSD

704 are shown in Fig. 9 and those corresponding to an initially wide DSD are shown in Fig. 10.

705 At an initially narrow DSD, the mean radius and the effective radius decrease with time in

706 agreement with the concept of homogeneous mixing. Formation of plateaus in the mean radii, in

707 the effective radii and in droplet dispersion over long time periods is caused by the existence of

708 droplets in the tail of DSD distributions. While the concentration of such droplets is negligibly

709 small, their evaporation takes a significant amount of time.

710 At an initially wide DSD (Fig.7b), complete evaporation of the smallest droplets starts at the

711 very beginning of the second stage of mixing. This evaporation leads to an increase in the

712 effective radius and in the mean radius that changes non-monotonically. An increase in the

713 value of the effective radius contradicts the concept of homogeneous mixing, according to which

714 both the mean radii and the effective radii decrease in the course of mixing. This increase is

715 explained by the fact that subsaturation at an initially wide DSD leads to a significant rapid

716 decrease in the concentration of small droplets, while the changes in LWC whose value is

717 determined by larger droplets, do not occur that quickly.

718 The opposite behaviors of the effective radii (as well as of the other characteristic droplet

719 sizes) at a narrow DSD vs. a wide DSD, illustrated in Figs. 9 and 10, suggest the existence of a

720 large number of DSDs with initial shapes at which the evaporation of droplets leads to a decrease

721 in droplet concentration, but does not change significantly the effective radius. So the constancy

722 of the effective radius at varying droplet concentrations does not allow to distinguish the mixing
723 type with full confidence. Even at a narrow DSD, the decrease in the value of the effective radius
724 does not exceed 20% at the an initial saturation deficit of 8.4 %.

725 In any case the evolution of DSD and of their parameters is determined by the competition
726 between two effects. First, this is the effect of partial droplet evaporation which shifts the DSD
727 toward smaller sizes and leads to a decrease in the mean radii and in the effective radii, as well
728 as widens the DSD. Second, this is the effect of complete evaporation of the smallest droplets,
729 which increases both the mean radii and the effective radii. The relative contribution of these two
730 effects depends on the initial DSD width and the value of the mean radius. The best indicators of
731 these two effects are the DSD width, σ and the DSD dispersion $\frac{\sigma}{\overline{r}}$.

732 At an initially narrow DSD and an initially low *RH*, partial evaporation initially dominates
733 and the DSD width increases due to the appearance of smaller droplets (Fig. 9c). Afterwards,
734 when complete droplet evaporation becomes the dominant factor, the DSD shifts significantly to
735 small sizes and the DSD width decreases. At an initially large *RH*, complete droplet evaporation
736 is not efficient, and the DSD gets continuously wider. Since the mean radius decreases, the DSD
737 dispersion tends to constant values at any initial *RH*. However, the largest DSD dispersion takes
738 place at an initially low *RH*, when evaporation substantially decreases the mean droplet radius.
739 As seen in Figs. 9d and 10d, the initial DSD dispersion at a narrow DSD is 0.1, while the initial
740 dispersion at a wide DSD is 0.5.

741 Figs. 10c and 10d show that at an initially wide DSD, homogeneous evaporation leads to an
742 increase in both DSD width and DSD dispersion. The increase in the DSD width indicates that
743 formation of the smallest droplets by partial evaporation is the main mechanism of the DSD
744 shape evolution. The DSD dispersion increases with time and rapidly reaches quasi-stationary
745 values of about 0.56 that are typical of real clouds.

746

747 **4.3. Evolution of LWC and of supersaturation**

748 Using Eq. (35), the time dependence of the liquid water mixing ratio is represented as

749 $$q(t)=\frac{4\pi\rho_w}{3\rho_a}N(t)\overline{r^3(t)}=\frac{4\pi\rho_w}{3\rho_a}\int\limits_{\sqrt{Q(t)}}^{\infty}\left(r_0^2-Q(t)\right)^{3/2}f_0(r_0)dr_0 \qquad (37)$$

750 If the initial DSD is approximated by a Gamma distribution, $q(t)$ can be written as

751 $$q(t)=\frac{4\pi\rho_w}{3\rho_a}\int\limits_{\sqrt{Q(t)}}^{\infty}\left(r_0^2-Q(t)\right)^{3/2}\frac{N_{m0}}{\Gamma(\alpha)\beta}\left(\frac{r_0}{\beta}\right)^{\alpha-1}\exp\left(-\frac{r_0}{\beta}\right)dr_0=$$
$$\frac{4\pi\rho_w}{3\rho_a}\frac{N_{m0}\beta^3}{\Gamma(\alpha)}\int\limits_{\eta(t)}^{\infty}\left(x^2-\eta^2(t)\right)^{3/2}(x)^{\alpha-1}\exp(-x)dx \qquad (38)$$

752 Since at $t=0$, $\eta=0$ and the initial liquid water mixing ratio is equal to

753 $q_{m0}=\frac{4\pi\rho_w}{3\rho_a}N_{m0}\beta^3\frac{\Gamma(\alpha+3)}{\Gamma(\alpha)}$, hence the normalized liquid water mixing ratio is calculated as

754 $$\frac{q(t)}{q_{m0}}=\frac{1}{\Gamma(\alpha+3)}\int\limits_{\eta(t)}^{\infty}\left(x^2-\eta^2(t)\right)^{3/2}(x)^{\alpha-1}\exp(-x)dx \qquad (39)$$

755

756 **Figure 11** shows the time dependencies of LWC for different initial RH_{m0} in the resulting
757 volume (Fig.11a: an initially narrow DSD; Fig.11b: an initially wide DSD). One can see that at
758 an initially narrow DSD the LWC rapidly decreases, either to zero (full evaporation) or, as in the
759 monodisperse case, to an equilibrium value during a time period of the phase relaxation time (see
760 Section 3 for comparison). At an initially wide DSD, the LWC decreases slowly and
761 monotonically. In general, at an initially narrow DSDs the time dependencies, $q_w(t)$ are quite
762 close to those for monodisperse DSD (Fig. 3b). The higher the initial *RH*, the smaller the change
763 in the LWC is.

764 To calculate the time dependencies of supersaturation, one can use the full equation (8) or
765 Eq. (15) written in the form:

766 $$S(t) = (S_{m0} + 1)\exp\left\{-A_2\left[q(t) - q_{m0}\right]\right\} - 1 \qquad (40)$$

767 In Eq. (40), S_{m0} and q_{m0} are the initial supersaturation and the liquid water mixing ratio,
768 respectively, at $t = 0$. The corresponding time dependencies are shown in **Figure 12.** The
769 analytical results of Eq. (40) are compared with the exact numerical solution obtained by a parcel
770 model, showing a good agreement. The behavior of supersaturation at a initially narrow DSD is
771 similar to that of a monodisperse DSD (Fig. 3a). As in Fig. 3a, the equilibrium non-zero values
772 of subsaturation correspond to complete droplet evaporation. At initially wide DSD, the
773 saturation deficit monotonically decreases as a consequence of the monotonic decrease in the
774 LWC.

775 **Figure 13** shows the dependencies of normalized LWC on normalized droplets
776 concentrations calculated at different values of the initial relative humidity RH_{m0} in the mixing
777 volume ((a): the initially narrow DSD and (b) the initially wide DSD). Each point on the curves
778 corresponds to a certain time. Since the dependencies are plotted in non-dimensional
779 coordinates, the time instance $t = 0$ corresponds to coordinates (1, 1). The numbers along the
780 curves denote the points corresponding to time instance $t = 20\,\text{s}$. At lower RH_{m0}, the curves
781 reach lower values of LWC and of droplet concentration. In case of an initially narrow DSD the
782 curve can be divided into three sections. The first section corresponds to high RH_{m0}
783 ($RH_{m0} > 90\%$). Within this section, the droplet concentration does not decrease with decreasing
784 LWC, which is in line with the conceptual scheme of homogeneous mixing (Fig. 1). This section
785 corresponds to the straight horizontal line in Fig. 8a. At lower relative humidity, the droplet
786 concentration begins to decrease with a decreasing LWC, in line with Fig. 8a. When the LWC
787 reaches small values, the dependence of the normalized LWC on the normalized droplet
788 concentration becomes close to linear. At an initially wide DSD (Fig. 13b), the dependence of

the LWC on droplet concentration is close to linear at all the values of RH_{m0}. This linear dependence means that the mean volume radius varies only slightly during droplet evaporation.

It is noteworthy that all the curves plotted for different initial values of RH_{m0} coincide. This coincidence can be explained by the fact that all the DSDs used depend on four parameters, namely, the three parameters of the initial Gamma distribution and on $Q(t)$ (Eq. 31). The parameters of Gamma distributions are identical for each panel in Fig. 13. Parameter $Q(t)$ monotonically increases with time. At different RH_{m0}, the values of $Q(t)$ reach the same values at different times. When the values of $Q(t)$ are the same, the DSDs and all the DSD moments are equal.

To sum up, at an initially narrow DSD and a comparatively large initial relative humidity $RH_{\mathrm{m0}} > 87\%$ phenomenon demonstrates properties typically attributed to homogeneous mixing, when a decrease in both the LWC and the effective radius takes place at unchanged droplet concentration (Figs. 8a, 9b, 11a, 13a). In contrast, in the case of an initially wide DSD, the evolution of the DSD and its moments is close to that typically attributed to inhomogeneous mixing, when droplet evaporation leads to a decrease in LWC and in droplet concentration, while the effective radius remains unchanged. During the changes of a wide DSD, its shape remains similar to itself (Fig. 7b), which is also considered typical of inhomogeneous mixing.

5. Discussion: Application of the concept of homogeneous mixing in numerical modeling

The procedure of mixing in any cloud model involves two steps. At the first step, the changes in microphysical values in each grid point are calculated using the turbulent flux divergences. In case mixing takes place between any two volumes represented by neighbouring grid points, the mixing volume containing both grid points never becomes homogeneous (*a fortiori*, the

813 microphysical values in these grid points do not become identical during one time step), so the
814 spatial gradients of the microphysical variables remain between neighbouring grid points. This
815 step represents inhomogeneous mixing at resolving scales. Mixing algorithm in models does not
816 operate with "final" equilibrium values, as assumed in the classical mixing concepts, but rather
817 with current time-dependent values. In contrast, the changes in the microphysical and
818 thermodynamical variables in the volumes represented by one grid points are often considered
819 uniform at each time step, and therefore, the modelled subgrid mixing is treated as
820 homogeneous. Therefore, in most numerical models mixing is inhomogeneous at resolved scales,
821 but homogeneous at subgrid scales.

822 The estimations in Tab. 1 indicate that mixing is homogeneous at scales lower than ~0.5 m.
823 This means that to simulate homogeneous mixing explicitly, the grid spacing should be less than
824 0.5 m. If such grid spacing is used, the separation between mixing types could be described
825 explicitly. However, grid spacing in most models significantly exceeds this value. This fact
826 brings up two questions: "What error is introduced when the spatial scale separating mixing
827 types in models is much larger than 0.5 m?" and "Why are spectral microphysics models with a
828 resolution of 40-50 m able to reproduce observed DSD and their moments with high accuracy
829 (Benmoshe et al., 2012; Khain et al., 2013, 2015; Magaritz-Ronen et al., 2014)?"

830 There are several factors that compensate errors in segregating mixing types in cloud models
831 and allow using grid scale $L > L_{pr}$ with little effect on DSD. The first factor is that mixing leads
832 to formation of cloud zones characterized by a spatial correlation scale (radius of correlation) of
833 temperature, humidity and droplet concentration of about 150-250 m (Magaritz-Ronen et al.,
834 2014). Numerical experiments with Lagrangian-Eulerian model of Sc (Magaritz-Ronen et al.,
835 2014) have shown that the results are not sensitive to the choice of parcel size, if this size is
836 substantially smaller than the spatial radius of correlation. Therefore, the mixing type has a
837 minor effect on the results of mixing at scales lower than the radius of correlation.

838 The second factor is that in-cloud mixing often takes place at conditions close to saturation.
839 At such high humidity, homogeneous and inhomogeneous mixing yield practically the same
840 results. The similarity of results for the two mixing types is due to the fact that mixing in clouds
841 is not accompanied by an appreciable phase transition.

842 The third factor was pointed out by Hill et al. (2009), who explained that stratocumulus cloud
843 evolution is insensitive to the type of sub-grid mixing since the rates of condensation/evaporation
844 caused by the resolved dynamics are by two orders of magnitude greater than the
845 condensation/evaporation rate caused by the sub-grid processes.

846 The fourth factor that permits us to treat sub-grid mixing as homogeneous near cloud
847 interfaces is that DSDs are polydisperse, which is opposite what is assumed in the conventional
848 mixing considerations. In the present study it was shown that for a broad DSD, the changes of
849 r_{eff} remain small during mixing. So, a relatively small partial evaporation of droplets provide
850 sufficient amount of water vapor for saturation of the volume. In this case homogeneous mixing
851 becomes indistinguishable from inhomogeneous. The saturation of the volume may be facilitated
852 by entrainment of water vapor from neighboring cloud volumes.
853

854 **6. Conclusions**

855

856 The present study is focused on the dynamics of DSD transformation during the evaporation
857 stage of homogeneous mixing. The results can be summarized as follows.
858 1. Analytical equations describing time evolution of normalized supersaturation and
859 normalized LWC are obtained. It is found that these time dependences are universal functions
860 of a sole non-dimensional parameter $\gamma = 1 + \frac{S_{m0}}{A_2 q_{m0}}$. In particular, the dependences of normalized
861 LWC at the final stage on the cloud air fraction, used for plotting the universal mixing diagrams,

862 are obtained analytically. These diagrams also depend on a sole non-dimensional parameter
863 $R = \frac{S_2}{A_2 q_1} < 0$, which is proportional to supersaturation in dry volume and inversely proportional
864 to liquid water mixing ratio in a cloud volume. This parameter is uniquely related with parameter
865 γ by Eq. (24). It is shown that in many cases the major changes in the LWC take place during
866 the time period of the order of the phase relaxation time τ_{pr}. The equilibrium state can be
867 reached after several τ_{pr} periods.

868 2. It is shown that the phase relaxation time is a natural time scale of mixing process. This is
869 clearly seen from the universal renormalized evaporation equations, in which the phase
870 relaxation time plays the role of a time unit. In some studies (e.g. Baker and Latham, 1979;
871 Burnet and Brenguier, 2007; Andejchuk et al., 2009) evaporation time for an individual droplet
872 under given sub-saturation is considered as a characteristic time of mixing. The present study
873 shows that only the phase relaxation time should be used as the characteristic time scale of
874 mixing since we have to consider the behavior of a large amount of droplets. Supersaturation (or
875 sub-saturation) is not a parameter that determines the phase relaxation time. Thus, the utilization
876 of the evaporation time of individual droplet (at unchanged supersaturation) as the characteristic
877 time scale of mixing is physically ungrounded. A strict relationship between the changes in
878 supersaturation and in the liquid water mixing ratio makes it impossible to consider the changes
879 in an individual droplet size and in supersaturation independently.

880 3. An important outcome of this study is demonstration of a significant difference in the
881 evaporative behavior between narrow DSD and wide DSD. It is shown that homogeneous
882 evaporation of a wide DSD is accompanied by reduction in LWC and in droplet concentration
883 due to total evaporation of small droplets. Such changes of LWC and droplet concentration are
884 qualitatively different from those in the classic concept of homogeneous mixing. As a result,
885 homogeneous mixing may be erroneously interpreted as inhomogeneous one.

4. It is shown that the evolution of DSDs and their moments in case of polydisperse DSDs, can qualitatively differ from that predicted by homogeneous mixing concept. Evaporation of a comparatively wide DSD may even lead to an increase in the effective radii and DSD high moments. This feature is typically attributed to inhomogeneous mixing.

Note that the role of DSD polydispersity in the mixing process is different from that in diffusion droplet growth in ascending parcels. In an ascending adiabatic parcel the supersaturation tends to zero with height, and the DSD width decreases with height as well. In this case, it is possible to reproduce the height dependencies and the time dependencies of supersaturation and of LWC using an "equivalent" monodisperse DSD with the same droplet concentration as a polydisperse DSDs (Pinsky et al., 2014). As regards to mixing with a polydisperse DSD, it cannot be reproduced using a monodisperse DSD, with a possible exception in case of an initially extremely narrow DSD.

Acknowledgements. This research was supported by the Israel Science Foundation (grant 1393/14), the Office of Science (BER), the US Department of Energy Award DE-SC0006788 and the Binational US-Israel Science foundation (grant 2010446). Dr. Korolev's participation was supported by Environment Canada.

Appendix A: List of Symbols

Table A1 here

910 **Appendix B. Derivation of closed equations for supersaturation and for liquid water**
911 **mixing ratio in the monodisperse DSD case.**

912

913 Let us consider motionless well-mixed adiabatic air volume having an initial supersaturation
914 $S_{m0} < 0$ and an initial liquid water mixing ratio q_{m0}.

915 1. Substitution of the formula of the liquid water mixing ratio $q = \frac{4\pi\rho_w}{3\rho_a} N r^3$ into the
916 equation for droplet radius evolution

917 $$r\frac{dr}{dt} = \frac{S}{F} \qquad \text{(B1)}$$

918 leads to the equation for the decrease of q with the time

919 $$\frac{dq}{dt} = \frac{3}{F}\left(\frac{4\pi\rho_w}{3\rho_a}\right)^{2/3} N^{2/3} S q^{1/3} = B N^{2/3} S q^{1/3} \qquad \text{(B2)}$$

920 where

921 $$B = \frac{3}{F}\left(\frac{4\pi\rho_w}{3\rho_a}\right)^{2/3} = const \qquad \text{(B3)}$$

922 2. Equation for supersaturation is written as (Korolev and Mazin, 2003)

923 $$\frac{1}{S+1}\frac{dS}{dt} = -A_2\frac{dq}{dt} \qquad \text{(B4)}$$

924 Integration of this equation under the assumption that $A_2 = const$ leads to the equation

925 $$\ln[S(t)+1] = -A_2 q(t) + C \qquad \text{(B5)}$$

926 where C is determined by initial conditions at $t = 0$

927 $$C = \ln(S_{m0}+1) + A_2 q_{m0} \qquad \text{(B6)}$$

928 Using Eqs. (B5) and (B6) one obtains the equation with respect to $S(t)$

929 $$S(t) = (S_{m0}+1)\exp\{-A_2[q(t) - q_{m0}]\} - 1 \qquad \text{(B7)}$$

930 3. Mutual substitution of Eqs. (B2) and (B7) leads to the closed differential equations for

931 $q(t)$ and $S(t)$

932 $$\frac{dq}{dt} = BN^{2/3}\left[(S_{m0}+1)\exp\{-A_2(q-q_{m0})\}-1\right]q^{1/3} \quad \text{(B8)}$$

933 $$\frac{1}{S+1}\frac{dS}{dt} = -A_2BN^{2/3}S\left(q_{m0} - \frac{1}{A_2}\ln\frac{S+1}{S_{m0}+1}\right)^{1/3} \quad \text{(B9)}$$

934 Eqs. (B8) and (B9) should be solved with initial conditions $q(0) = q_{m0}$ and $S(0) = S_{m0}$

935 respectively.

936 4. In case $|S_{m0}| << 1$, supersaturation is close to zero all the time $|S(t)| << 1$ and Eqs. (B7-B9)

937 can be simplified as follows

938 $$S(t) = S_{m0} - A_2\left[q(t) - q_{m0}\right] \quad \text{(B10)}$$

939 $$\frac{dq}{dt} = -BN^{2/3}\left(A_2q^{4/3} - (A_2q_{m0} + S_{m0})q^{1/3}\right) \quad \text{(B11)}$$

940 $$\frac{dS}{dt} = -B(A_2N)^{2/3}(A_2q_{m0} + S_{m0} - S)^{1/3}S \quad \text{(B12)}$$

941

942 5. Then one can obtain Eqs. (B10-B12) in a non-dimensional form. Let us define time scale

943 $\tau_{m0} = \left(BA_2N^{2/3}q_{m0}^{1/3}\right)^{-1}$, normalized liquid water mixing ratio $\tilde{q} = \frac{q}{q_{m0}}$, normalized supersaturation

944 $\tilde{S} = \frac{S}{A_2q_{m0}}$, and non-dimensional time $\tilde{t} = t/\tau_{m0} = BA_2N^{2/3}q_{m0}^{1/3}t$. The Eqs. (B10-B12) can be

945 rewritten in a non-dimensional form as

946 $$\tilde{S}(\tilde{t}) = -\tilde{q}(\tilde{t}) + \gamma \quad \text{(B13)}$$

947 $$\frac{d\tilde{q}}{d\tilde{t}} = \tilde{q}^{1/3}\left(\gamma - \tilde{q}\right) \quad \text{(B14)}$$

948 $$\frac{d\tilde{S}}{d\tilde{t}} = -(\gamma - \tilde{S})^{1/3}\tilde{S} \quad \text{(B15)}$$

where non-dimensional parameter $\gamma = 1 + \frac{S_{m0}}{A_2 q_{m0}}$ depends on initial supersaturation S_{m0} and initial liquid water mixing ratio q_{m0}. Eq. (B14) should be solved with initial condition $\tilde{q}(0) = 1$ and Eq. (B15) should be solved with initial condition $\tilde{S}(0) = \frac{S_{m0}}{A_2 q_{m0}} < 0$. Note that Eqs. (B14) and (B15) are rigidly connected by Eq. (B13).

References

Andejchuk, M., Grabowski, W. W., Malinowski, S. P., and Smolarkiewicz, P. K.: Numerical simulation of cloud–clear air interfacial mixing: homogeneous vs. inhomogeneous mixing., *J. Atmos. Sci.*, **66**, 2493–2500, 2009.

Anthes, R.A.,: Tropical cyclones-Their evolution, structure, and effects. Monograph 41, Amer. Meteorol. Soc., 208 pp, 1982

Baker, M., and J. Latham: The evolution of droplet spectra and the rate of production of embyonic raindrops in small cumulus clouds. *J. Atmos. Sci.*, **36,** 1612–1615, 1979.

Baker, M., R. G. Corbin, and J. Latham: The influence of entrainment on the evolution of cloud drop spectra: I. A model of inhomogeneous mixing. *Quart. J. Roy. Meteor. Soc.*, **106,** 581–598, 1980.

Baker M. B. and J. Latham: A diffusive model of the turbulent mixing of dry and cloudy air. *Quart. J. R. Met.* Soc., **108**, 871-898, 1982

Bar-Or R. Z., I. Koren, O. Altaratz and E. Fredj: Radiative properties of humidified aerosol in cloudy environment. *Atmos. Res.*, **118**, 280–294, 2012.

Benmoshe, N., M. Pinsky, A. Pokrovsky, and A. Khain: Turbulent effects on the microphysics and initiation of warm rain in deep convective clouds: 2-D simulations by a spectral mixed-phase microphysics cloud model. *J. Geophys. Res.*, **117**, 1–20, 2012.

Benmoshe N., M. Pinsky, A. Pokrovsky and A. Khain: Turbulent effects on microstructure and precipitation of deep convective clouds as seen from simulations with a 2-D spectral microphysics cloud model. *J. Geop. Res*., **117**, D06220, 2012.

Blyth, A. M., Choularton, T. W., Fullarton, G., Latham, J., Mill, C. S., Smith, M. H., and Stromberg, I. M.: The Influence of entrainment on the evolution of cloud droplet spectra. 2. Field experiments 5 at Great Dun Fell, *Q. J. Roy. Meteor. Soc*., **106**, 821–840, 1980.

Burnet, F., and J-L. Brenguier: Observational study of the entrainment-mixing process in warm convective clouds. *J. Atmos. Sci.*, **64,** 1995–2011, 2007.

Denvich B. J., P. Bartello, J-L. Brenguier, L.R. Collins, W.W. Grabowski, R.H.A. Ijzermans, S.P. Malinovski, M.W. Reeks, J.C. Vassilicos, L-P. Wang, and Z. Warhaft: Droplet growth in warm turbulent clouds. *Q. J. Roy. Meteorol. Soc.,* **138**, 1401-1429, 2012.

Dimotakis P. E.: Turbulent mixing, *Annu. Rev. Fluid Mech*., **37**, 329-356, 2005.

Ferrier, B.S. and R.A. Houze: One-dimensional time dependent modeling of GATE cumulonimbus convection. *J. Atmos. Sci.,* **46**, 330-352, 1989.

Gerber H, Frick G, Jensen J.B, and Hudson J.G.: Entrainment, mixing, and microphysics in trade-wind cumulus. *J. Meteorol. Soc. Jpn.,* **86A**. 87-106, 2008.

Ghan S. J., Hayder Abdul-Razzak, A. Nenes, Yi Ming, Xiaohong Liu, M. Ovchinnikov, B. Shipway, N. Meskhidze, Jun Xu and X. Shi: Droplet nucleation: Physically-based parameterizations and comparative evaluation, *J. Adv. Model. Earth Syst*., 3, M10001, 33 pp. DOI:10.1029/2011MS000074, 2011.

Goix P. J. and L. Talbot: Turbulent counter flow diffusion flame structure and dilution effects combustion. *Science and Technology*, 79, #4-6, 1991.

Hill, A. A., G. Feingold, and H. Jiang: The influence of entrainment and mixing assumption on aerosol–cloud interactions in marine stratocumulus. *J. Atmos. Sci.*, 66, 1450–1464, 2009.

Jeffery, C. A.: Inhomogeneous cloud evaporation, invariance, and Damköhler number. J. Geophys. Res. 112, D24S21, doi:10.1029/2007JD008789

Kerstein A. R.: Linear eddy modelling of turbulent scalar transport and mixing, *Comb. Sci. Technol*., 60, 391-421, 1988.

Kerstein A. R.: Linear-eddy modelling of turbulent transport. Part 6. Microstructure of diffusive scalar mixing fields. *J. Fluid Mech*., **231**, 361-394, 1991.

Khain A., Thara V. Prabha, Nir Benmoshe, G. Pandithurai, M. Ovchinnikov: The mechanism of first raindrops formation in deep convective clouds. *J. Geophys. Res.* Atmospheres**. 118**, 9123–9140, 2013.

Khain A.P. , K. D. Beheng, A. Heymsfield, A. Korolev, S.O. Krichak, Z. Levin, M. Pinsky, V. Phillips, T. Prabhakaran, A. Teller, S.C. van den Heever, J.-I. Yano: Representation of microphysical processes in cloud-resolving models: spectral (bin) microphysics vs. bulk parameterization. *Review of Geophysics* (in press) , 2015

Knight C. A. and L. J. Miller: Early radar echoes from small, warm cumulus: Bragg and hydrometeor scattering. *J. Atmos. Sci.*, **55**, 2974-2992, 1998.

Korn G. A. and T. M. Korn: Mathematical handbook for scientists and engineers: Definitions, theorems, and formulas for reference and review. Courier Corporation – Mathematics - 1130 pp, 2000.

Korolev, A.V.: The influence of suresaturation fluctuations on droplet size spectra formation. *J. Atmos. Sci.*, **52**, 3620-3634, 1995.

Korolev, A. V., and G. A. Isaac: Drop growth due to high supersaturation caused by isobaric mixing. *J. Atmos. Sci.*, **57,** 1675–1685, 2000.

Korolev A., V, Isaac, G. A.: Phase transformation of mixed-phase clouds. *Q. J. Roy. Meteorol. Soc*. **129**, 19-38, 2003.

1020 Korolev, A. V., and I. P. Mazin: Supersaturation of water vapor in clouds. *J. Atmos. Sci.*, **60,**
1021 2957–2974, 2003.
1022 Korolev A., A. Khain, M. Pinsky, and J. French: Theoretical investigation of mixing in warm
1023 clouds. Part 1: Classical concept. Submitted, 2015
1024 Kumar B, J. Schumacher, and R. A. Shaw: Cloud microphysical effects of turbulent mixing
1025 and entrainment. *Theor. Comput. Fluid Dyn.*, **27**, 361–376, 2013.
1026 Latham, J. and Reed, R. L.: Laboratory studies of effects of mixing on evolution of cloud
1027 droplet spectra, *Q. J. Roy. Meteor. Soc*., **103**, 297–306, 1977.
1028 Lehmann, K., H. Siebert, R. A. Shaw: Homogeneous and inhomogeneous mixing in cumulus
1029 clouds: Dependence on local turbulence structure. *J. Atmos. Sci.*, **66**, 3641–3659, 2009.
1030 Mazin, I. P.: Effect of phase transition on formation of temperature and humidity
1031 stratification in clouds. *Proc. Int. Conf. on Cloud Physics.* Toronto, Ontario, Canada, Amer.
1032 Meteor. Soc., 132– 137, 1968.
1033 Magaritz-Ronen L., M. Pinsky, and A. Khain: Effects of turbulent mixing on the structure
1034 and macroscopic properties of stratocumulus clouds demonstrated by a Lagrangian trajectory
1035 model. *J. Atmos. Sci.,* **71**, 1843–1862, 2014.
1036 Monin, A.S. and Yaglom, A.M.: "Statistical Fluid Mechanics: Mechanics of Turbulence",
1037 vol. **2**, MIT Press. 911 pp., 1975.
1038 Pinsky, M. and A. P. Khain: Effects of in-cloud nucleation and turbulence on droplet
1039 spectrum formation in cumulus clouds. *Quart. J. Roy. Meteorol. Soc*., **128**, 1–33, 2002.
1040 Pinsky M., I.P. Mazin, A. Korolev, and A. Khain: Supersaturation and diffusional drop
1041 growth in liquid clouds, *J. Atmos. Sci.*, **70**, 2778-2793, 2013.
1042 Pinsky M., I. P. Mazin, A. Korolev and A. Khain: Supersaturation and diffusional droplet
1043 growth in liquid clouds: Polydisperse spectra. *J. Geophys. Res., Atmospheres,* **119**, 12,872–
1044 12,887, 2014

Pruppacher, H.R., Klett, J.D.: Microphysics of clouds and precipitation. 2nd edn. Oxford Press, 914 p. , 1997

De Rooy, W. C., P. Bechtold, K. Fröhlich, C. Hohenegger, H. Jonker, D. Mironov, A. P. Siebesma, J. Teixeira and J-I Yano: Entrainment and detrainment in cumulus convection: an overview, *Q. J. Royal Met. Soc*., **139**, 1–19, 2013.

Stull, Roland B.: An Introduction to Boundary Layer Meteorology. Springer, Netherlands, 666 pp, 1988.

Troen, I. and L. Mahrt: A simple model of the atmospheric boundary layer: Sensitivity to surface evaporation. *Boundary Layer Met.* **37**, 129-148, 1986.

Warhaft Z.: Passive scalars in turbulent flows. *Annu. Rev. Fluid Mech*., **32**, 203–240, 2000.

Warner J.: The microstructure of cumulus cloud. Part 1: general features of the droplet spectrum, *J. Atmos. Sci.*, **26**, 1049-1059, 1969.

1059

1060 **Table 1.** Linear scales of volumes experiencing homogeneous mixing at conditions typical of

1061 different cloud types.

Cloud type	N, cm^{-3}	LWC gm^{-3}	r, μm	Dissipation rate, cm^2/s^3	Phase relaxation time, s	Phase scale, m
Maritime Convective	100	2.0	16.8	300	2.01	0.49
Maritime Stratocumulus	100	0.5	10.6	10	3.19	0.18
Weak Stratocumulus	100	0.2	7.8	5	4.33	0.2
Continental Convective	500	2	8.0	500	0.75	0.6

1062

1063

1064

1065 **Table 2** Estimations of mixing results at different environmental conditions*

T (^{o}C)	A_2	q_1, g/kg	RH_2 %	μ (cloud fraction)	$R\frac{1-\mu}{\mu}$	Result of mixing
$T = 0^oC$	400	1.0	95	0.5	-0.125	cloudy
$T = 0^oC$	400	1.0	50	0.5	-1.25	Non-cloudy
-10^oC	700	2.0	95	0.5	-0.036	cloudy
-10^oC	700	2.0	50	0.5	-0.36	cloudy
-20^oC	1500	2.0	95	0.5	-0.017	cloudy
-20^oC	1500	2.0	50	0.5	-0.17	cloudy
-20^oC	1500	2.0	95	0.1	-0.153	cloudy
-20^oC	1500	2.0	50	0.1	-1.53	Non-cloudy

1066 * The values A_2 are estimated as proposed by Pinsky et al., (2013).

1067

1068

1069 **Tab.3** Parameters of the initial Gamma distributions

DSD	N_{m0}, cm^3	α	β, μm	Modal radius, μm	LWC, g/m^3
Narrow	264.2	101.0	0.1	10.0	0.587
Wide	71.0	4.3	3.1	10.0	0.587

1070

1071

1072

1073 **Tab. A1. List of symbols**

1074

Symbol	Description	Units
A_2	$\frac{1}{q_v}+\frac{L^2}{c_p R_v T^2}$, coefficient	nd
B	$\frac{3}{F}\left(\frac{4\pi\rho_w}{3\rho_a}\right)^{2/3}$, coefficient	$m^2\ s^{-1}$
C	constant of integration	nd
c_p	specific heat capacity of moist air at constant pressure	$J\ kg^{-1}K^{-1}$
$\mathscr{D}$	coefficient of water vapour diffusion in the air	$m^2\ s^{-1}$
e	water vapor pressure	$N\ m^{-2}$
e_S	saturation vapour pressure above a flat water surface	$N\ m^{-2}$
F	$F=\frac{\rho_w L^2}{k_a R_v T^2}+\frac{\rho_w R_v T}{e_S(T)\mathscr{D}}$, coefficient	$m^{-2}\ s$
$f(r,t)$	droplet size distribution	m^{-4}
$f_0(r_0)$	droplet size distribution after the first stage of mixing	m^{-4}
k_a	coefficient of air heat conductivity	$J\ m^{-1}s^{-1}K^{-1}$
L_{mix}	characteristic spatial scale of mixing	m
L_{pr}	spatial scale of phase relaxation	m
L	latent heat for liquid water	$J\ kg^{-1}$
N	droplet concentration	m^{-3}
N_1	droplet concentration in a cloud volume	m^{-3}
N_{m0}	droplet concentration after the first stage of mixing	m^{-3}
p	pressure of moist air	$N\ m^{-2}$
q	liquid water mixing ratio	kg/kg
q_1	liquid water mixing ratio in a cloudy volume	kg/kg
q_{m0}	liquid water mixing ratio after the first stage of mixing	kg/kg
q_w	liquid water content (LWC)	gm^{-3}

q_{w0}	LWC after the first stage of mixing	gm^{-3}
q_v	water vapor mixing ratio	kg/kg
$\tilde{q}$	normalised liquid water mixing ratio equal to normalized LWC	nd
$\tilde{q}_{\min}$	normalized equilibrium liquid water mixing ratio equal to normalized equilibrium LWC	nd
Q	change of square of droplet radius	m^2
r	droplet radius	m
R	$\frac{S_2}{A_2 q_1}$	nd
R_a	specific gas constant of moist air	$J\ kg^{-1}K^{-1}$
R_v	specific gas constant of water vapor	$J\ kg^{-1}K^{-1}$
S	$e/e_w - 1$, supersaruration over water	nd
S_{m0}	supersaturation after the first stage of mixing	nd
S_2	supersaturation in a dry volume	nd
$\tilde{S}_{\max}$	maximal normalized supersaturation	nd
$\tilde{S}$	normalized supersaturation	nd
T	temperature	K
T_1	temperature in a cloud volume	K
T_2	temperature in a dry volume	K
t_e	normalized evaporation time	nd
t	time	s
$\tilde{t}$	non-dimensional time	nd
$x(\tilde{t})$	non-dimensional variable	nd
α	parameter of the Gamma distribution	nd
β	parameter of the Gamma distribution	m^{-1}
χ	$\gamma^{1/3}$, non-dimensional parameter	nd
ε	turbulent dissipation rate	m^2s^{-3}
γ	$1+\frac{S_{m0}}{A_2 q_{m0}}$, non-dimensional parameter	nd

δq_m	mixing ratio of liquid water required to saturate 1 kg of the cloud (or cloudy?) volume after instant mixing	nd
μ	mass fraction of cloud air	nd
ρ_a	air density	kg m^{-3}
ρ_w	density of liquid water	kg m^{-3}
τ_{pr}	phase relaxation time	s
τ_{mix}	characteristic time of mixing	s
τ_{m0}	time scale	s

"nd" denotes non-dimensional

Figures

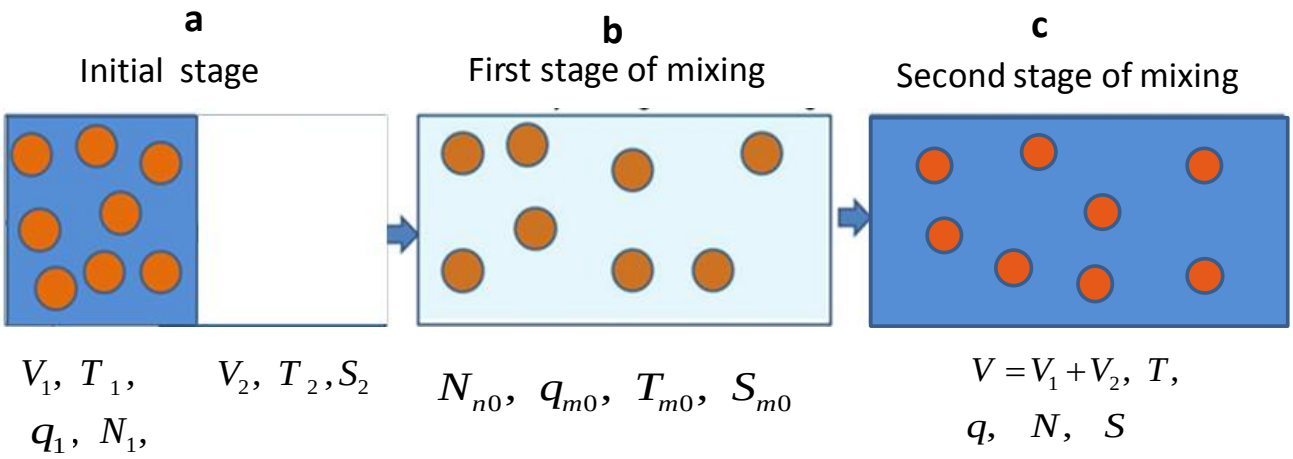

Fig. 1. Conceptual scheme of homogeneous mixing in case of monodisperse DSD. The subsaturated volume of dry air is colored white, and the cloudy volumes with saturated air are colored dark blue. The volume forming as a result of mixing after total homogenization is colored light blue. Index 1 shows the initial values characterizing the initially cloudy volume. Index 2 denotes initial values in the droplet-free volume. Index "$m0$" denotes values in the mixing volume after the first stage of mixing.

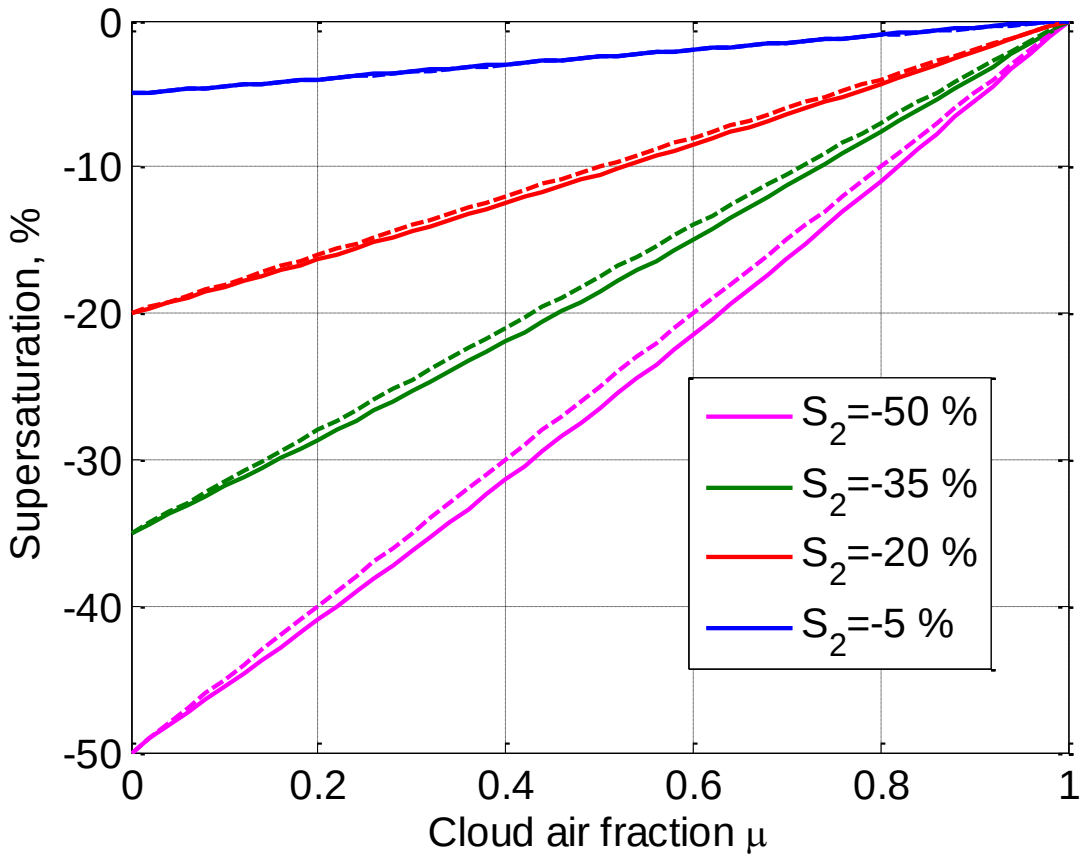

Fig. 2. Dependence of supersaturation on parameter μ: simulation results (solid line) and an approximate linear dependence calculated using Eq. (6b) (dashed line). The initial temperatures of two volumes are $T_1 = 8\,^{o}\mathrm{C}$ and $T_2 = 10\,^{o}\mathrm{C}$.

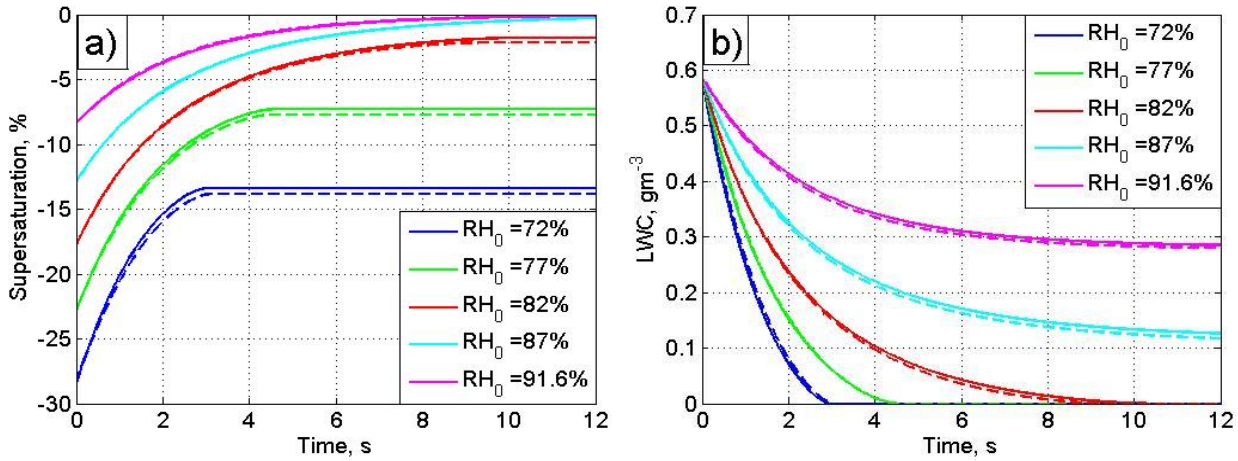

Fig. 3. Dependencies $S(t)$ (a) and $q_w(t)$ (b), calculated at different initial relative humidity RH_{m0} using closed differential equations (12,13) (solid lines) and using a parcel model (dashed lines). The calculation parameters are $T_{m0} = 10^{o}C$, $p_0 = 842$ mb, $r_0 = 10\ \mu m$, $N_{m0} = 140\ cm^{-3}$, $q_{w0} = 0.58\ gm^{-3}$.

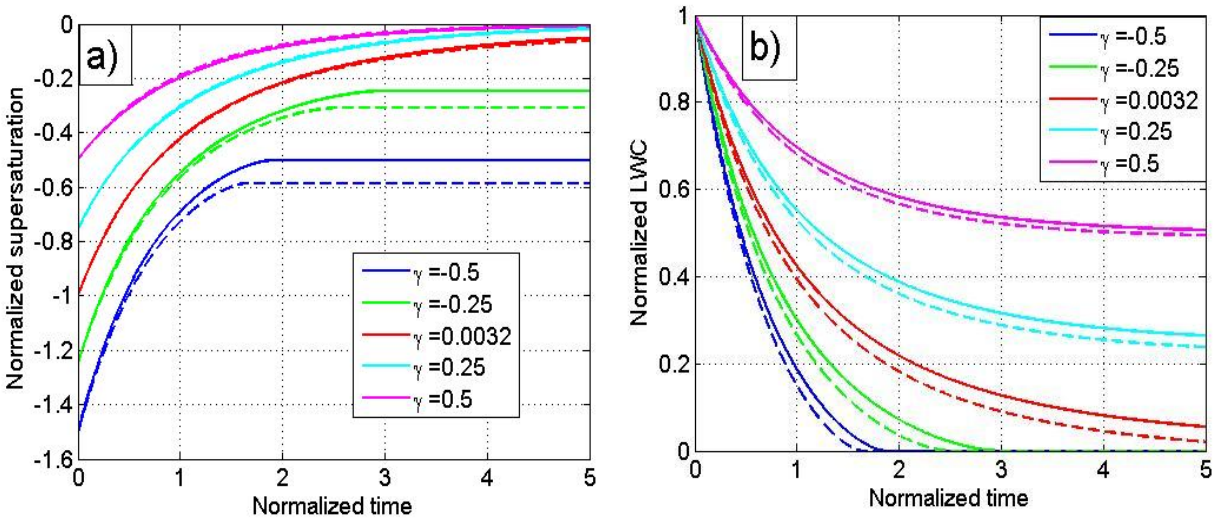

Fig. 4. Universal dependencies $\tilde{S}(\tilde{t})$ (a) and $\tilde{q}(\tilde{t})$ (b), calculated at different values of parameter γ using Eqs. (17-18) (solid lines) and using a parcel model (dashed lines).

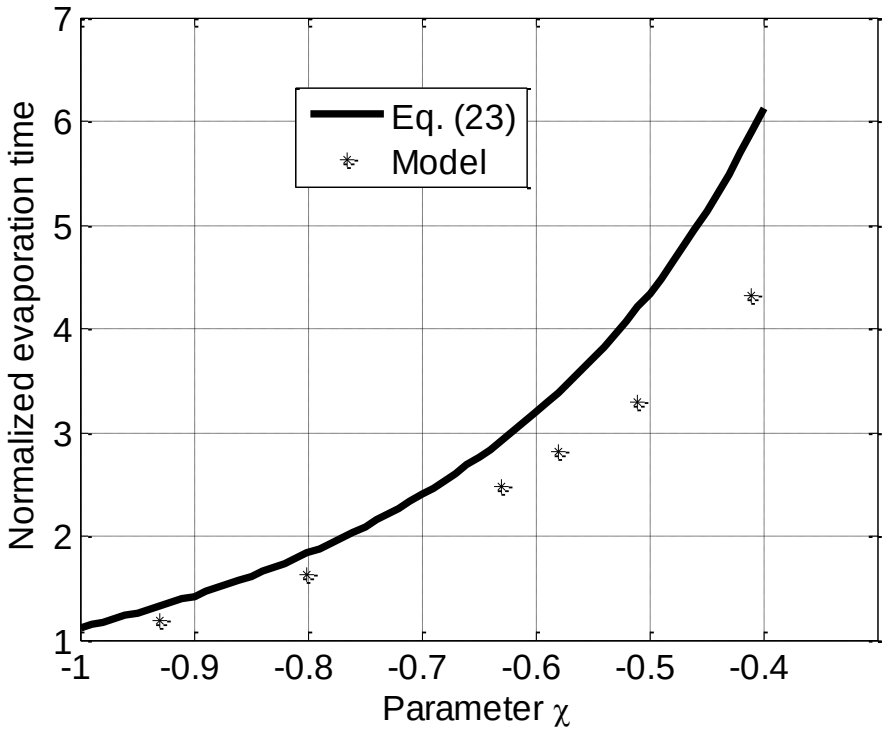

Fig. 5. Dependence of the evaporation time on parameter χ, $t_e(\chi)$. Time is measured at the relaxation time scales. The values obtained using a parcel model are shown by asterisks.

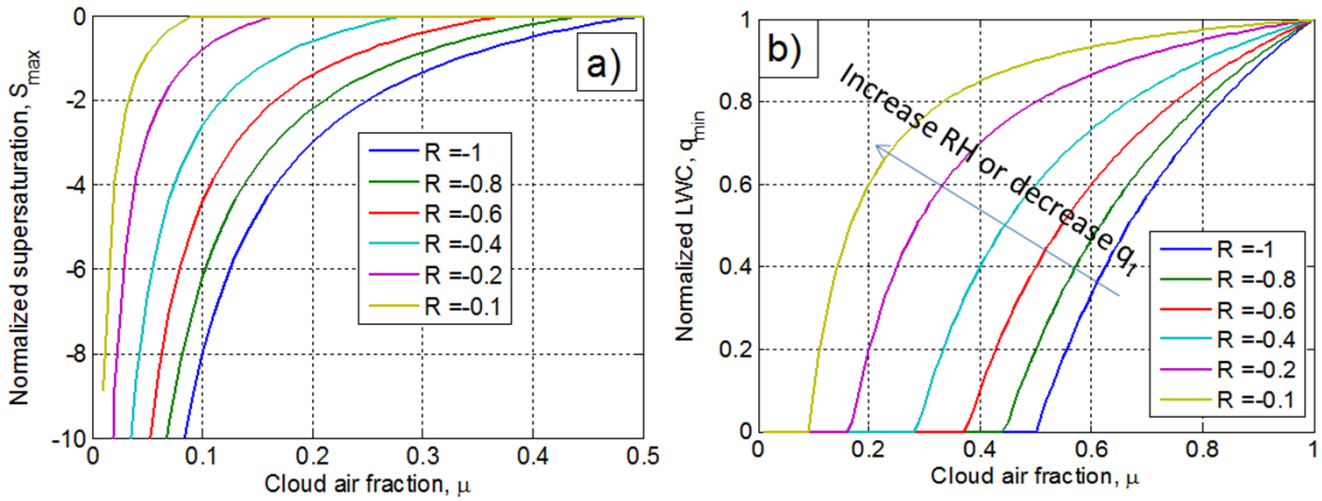

Fig. 6. Dependencies of normalized equilibrium supersaturation $\tilde{S}_{max}$ (a) and normalized equilibrium LWC (which is equal to normalized equilibrium liquid water mixing ratio) $\tilde{S}_{max}$ (b) on cloudy air fraction at the final stage of homogeneous mixing. Curves of different colors correspond to different values of non-dimensional parameter $R = \frac{S_2}{A_2 q_1}$.

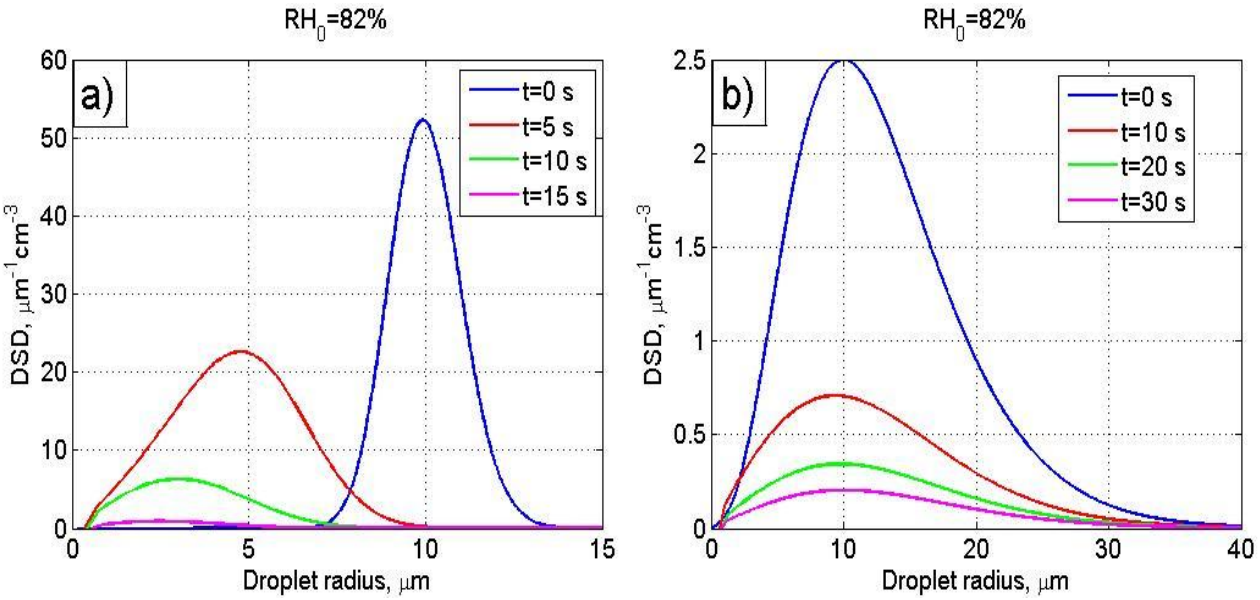

Fig. 7. Time evolution of an initially narrow DSD (a) and an initially wide DSD (b). The initial calculation parameters are the same in both examples: $T_{m0} = 10\ ^{\circ}C$, $p = 829$ mb, $RH_{m0} = 82$ % and $q_{w0} = 0.587$ g/m^3. The parameters of the initial Gamma distributions are given in Tab. 3.

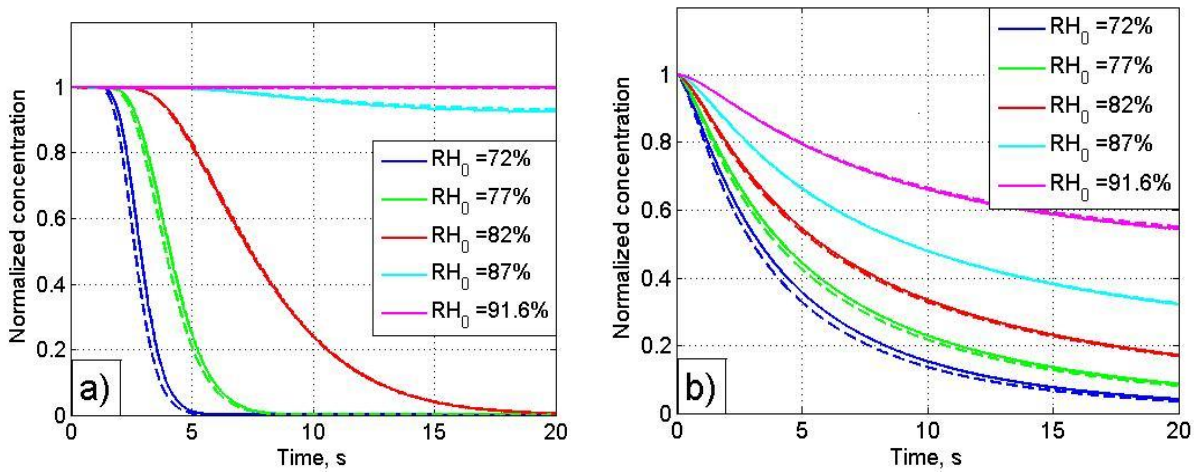

Fig.8. Time dependencies of normalized droplet concentration for an initially narrow DSD (a) and an initially wide DSD (b) at initially different values of RH_{m0} in the resulting volume. The dependencies are calculated directly using a parcel model (solid lines) and using Eq. (33) (dashed lines). The thermodynamic parameters are the same as in Fig.7. Parameters of the initial DSDs are given in Tab. 3.

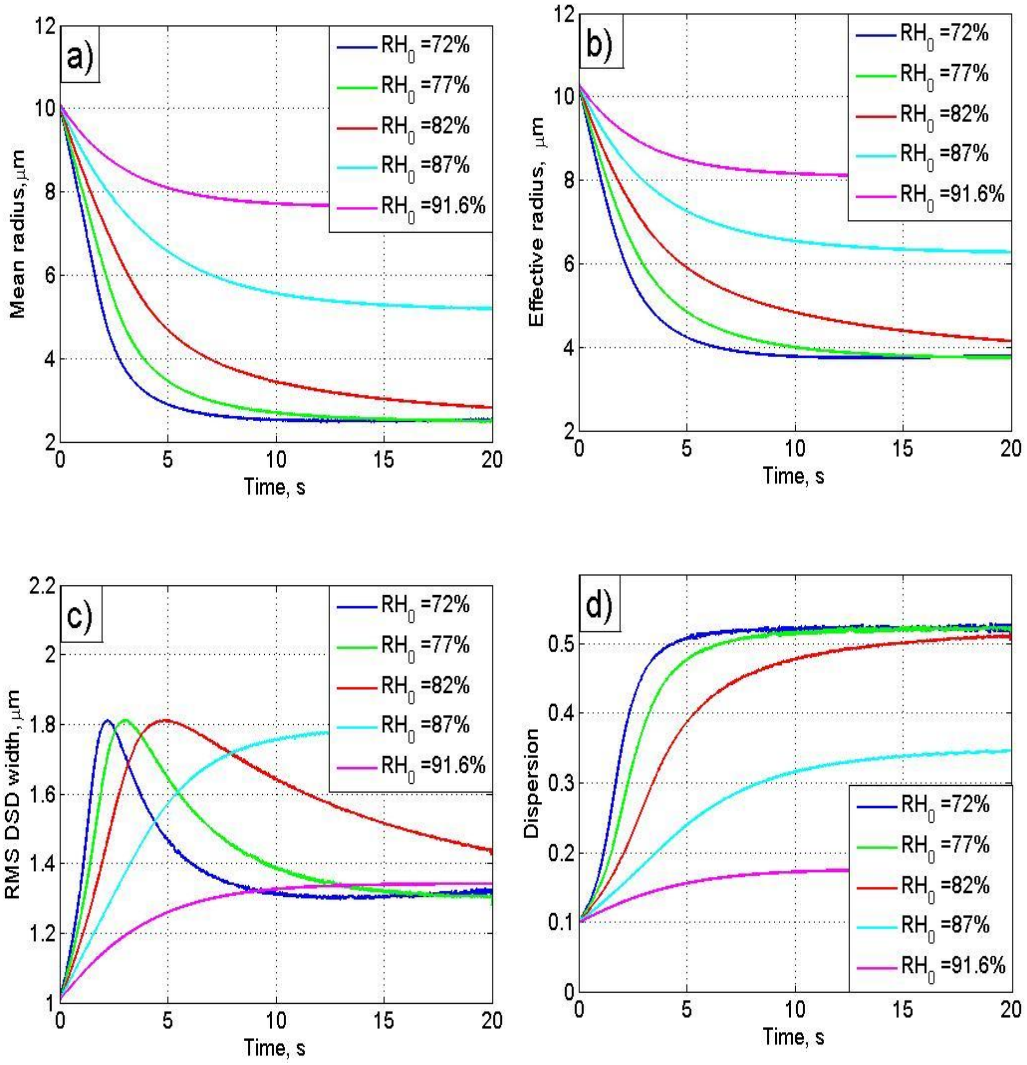

Fig. 9. Dependencies of moment functions typically used for characterizing DSD shape at different values of the initial relative humidity RH_{m0} in the resulting volume. The dependencies are calculated using a parcel model for an initially narrow DSD (Tab. 3). The thermodynamic parameters are the same as in Fig. 7.

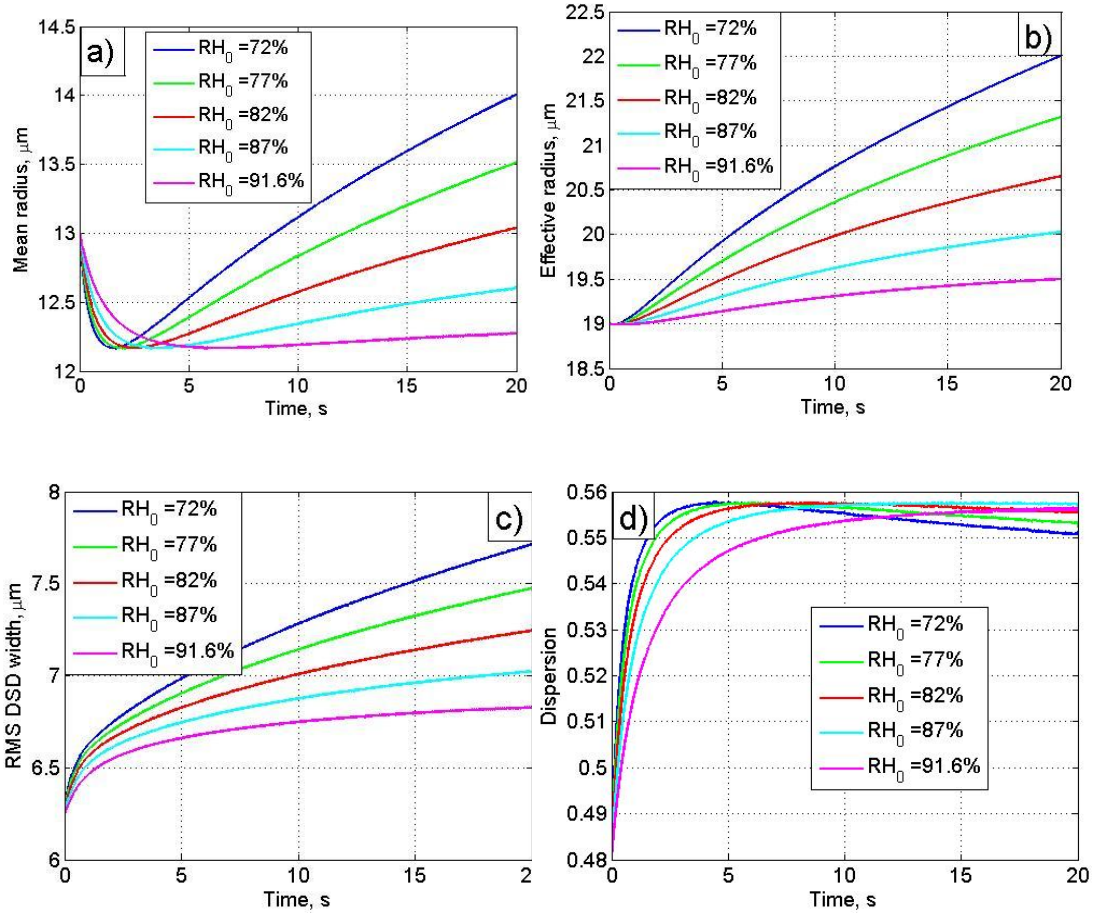

Fig. 10. The same as in Fig. 9 but for an initially wide DSD.

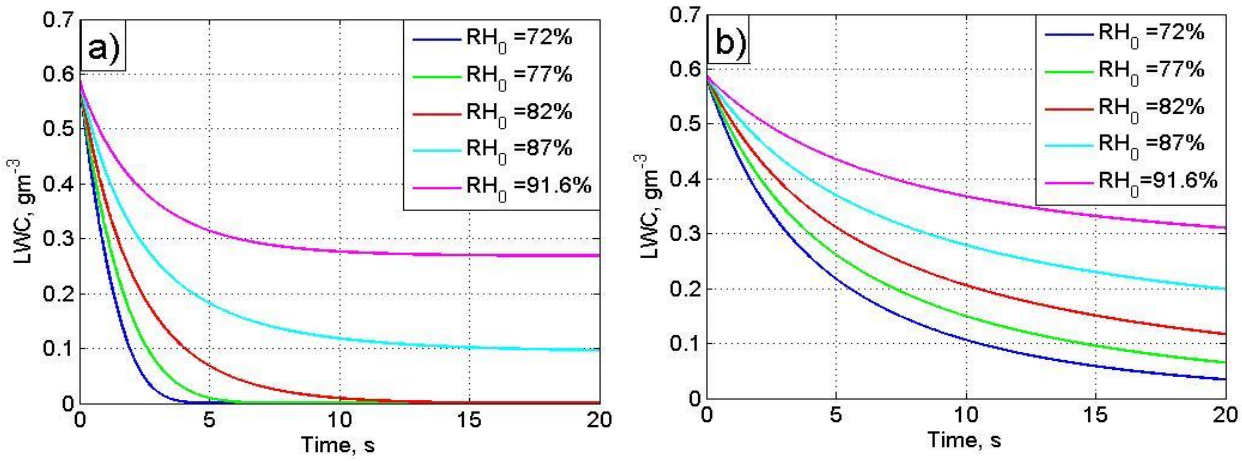

Fig. 11. Time dependencies of LWC calculated using a parcel model at different values of RH_{m0} in the resulting volume, for an initially narrow DSD (a) and an initially wide DSD (b). The thermodynamic parameters are the same as in Fig.7. The parameters of the initial DSDs are given in Tab. 3.

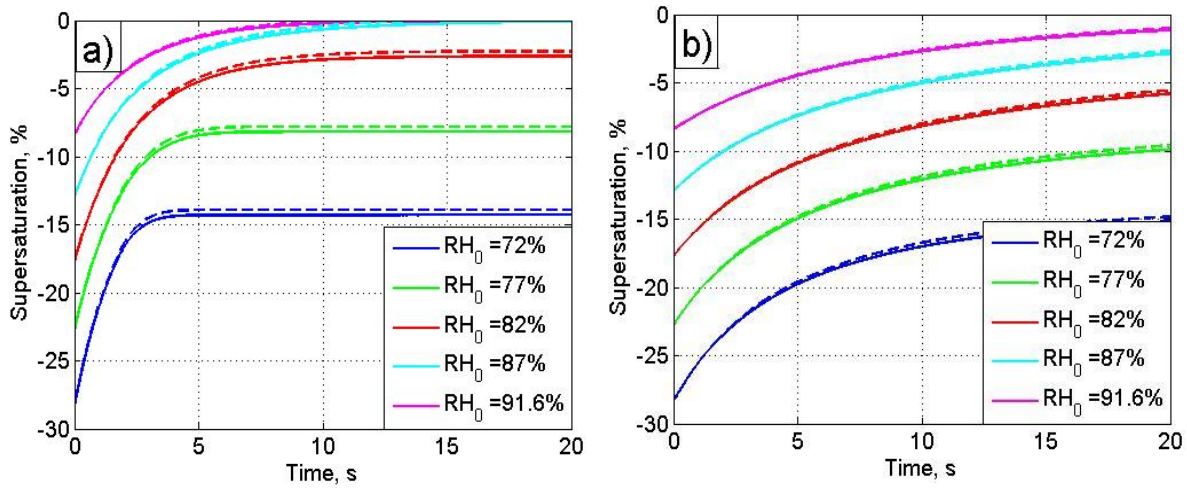

Fig. 12. Time dependencies of supersaturation calculated at different values of the initial relative humidity RH_{m0} in the resulting volume, using Eq. (8) (solid lines) and Eq. (40) (dashed lines), for an initially narrow DSD (a) and an initially wide DSD (b). The thermodynamic parameters are the same as in Fig.7. The parameters of the initial DSDs are given in Tab.3.

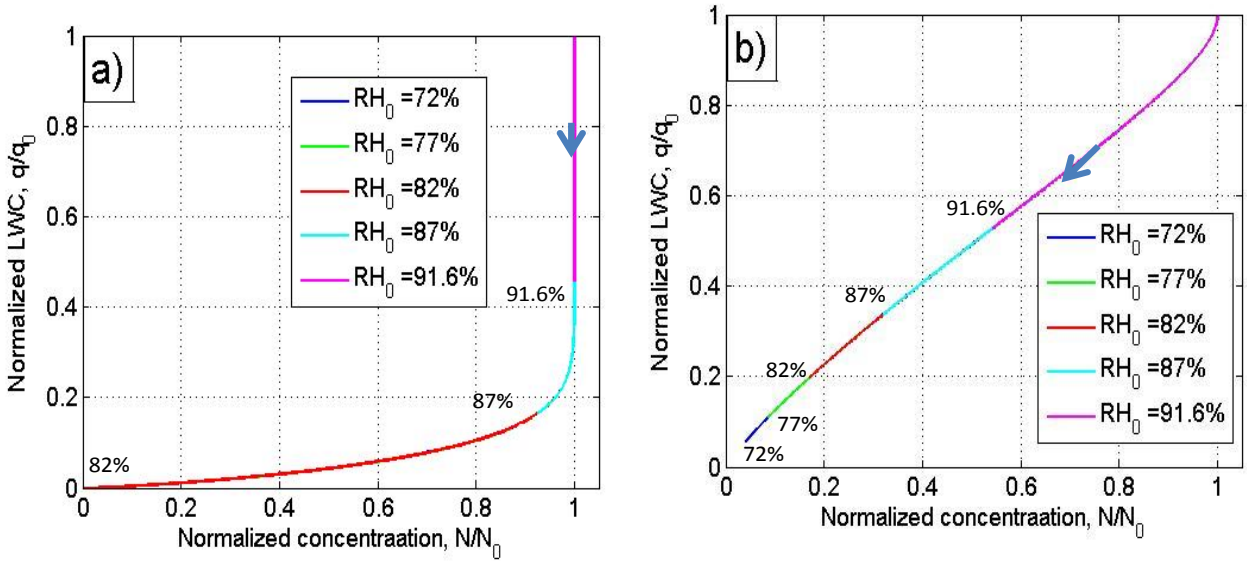

Fig. 13. Dependencies of normalized LWC on the normalized number concentration of droplets calculated at different values of the initial relative humidity RH_{m0} in the resulting volume, for an initially narrow DSD (a) and an initially wide DSD (b). The thermodynamic parameters are the same as in Fig.7. The parameters of the initial DSDs are given in Tab. 3. Arrows denote the direction of increasing time.